Gondwana Research 28 (2015) 1344–1360

Contents lists available at ScienceDirect

Gondwana Research

journal homepage: www.elsevier.com/locate/gr

Density heterogeneity of the cratonic lithosphere: A case study of the Siberian Craton

Y. Cherepanova *, I.M. Artemieva

Geology Section, IGN, University of Copenhagen, Denmark

ARTICLE INFO

Article history:
Received 22 August 2014
Received in revised form 7 October 2014
Accepted 22 October 2014
Available online 30 October 2014

Handling Editor: M. Santosh

Keywords:
Mantle depletion
Isopycnicity
Melt-metasomatism
Intracratonic basins
Kimberlites

ABSTRACT

Using free-board modeling, we examine a vertically-averaged mantle density beneath the Archean–Proterozoic Siberian Craton in the layer from the Moho down to base of the chemical boundary layer (CBL). Two models are tested: in Model 1 the base of the CBL coincides with the LAB, whereas in Model 2 the base of the CBL is at a 180 km depth. The uncertainty of density model is <0.02 t/m^3 or <0.6% with respect to primitive mantle. The results, calculated at in situ and at room temperature (SPT) conditions, indicate a heterogeneous density structure of the Siberian lithospheric mantle with a strong correlation between mantle density variations and the tectonic setting. Three types of cratonic mantle are recognized from mantle density anomalies. 'Pristine' cratonic regions not sampled by kimberlites have the strongest depletion with density deficit of 1.8–3.0% (and SPT density of 3.29–3.33 t/m^3 as compared to 3.39 t/m^3 of primitive mantle). Cratonic mantle affected by magmatism (including the kimberlite provinces) has a typical density deficit of 1.0–1.5%, indicative of a metasomatic melt-enrichment. Intracratonic sedimentary basins have a high density mantle (3.38–3.40 t/m^3 at SPT) which suggests, at least partial, eclogitization. Moderate density anomalies beneath the Tunguska Basin imply that the source of the Siberian LIP lies outside of the Craton. In situ mantle density is used to test the isopycnic condition of the Siberian Craton. Both CBL thickness models indicate significant lateral variations in the isopycnic state, correlated with mantle depletion and best achieved for the Anabar Shield region and other intracratonic domains with a strongly depleted mantle. A comparison of synthetic Mg# for the bulk lithospheric mantle calculated from density with Mg# from petrological studies of peridotite xenoliths from the Siberian kimberlites suggests that melt migration may produce local patches of metasomatic material in the overall depleted mantle.

1. Introduction

The Siberian Craton occupies a significant part of northern Eurasia and is one of the largest Archean–Proterozoic regions (Fig. 1a). Its tectonic structure is very heterogeneous and includes the Archean–Paleoproterozoic terranes separated by Proterozoic suture zones. Parts of the Craton were reworked in Phanerozoic by rifting and several pulses of magmatic activity, followed by differentiated subsidence with the formation of intracratonic basins (Fig. 1b).

Similar to other cratons worldwide, the Siberian Craton is underlain by a thick lithospheric mantle, which may reach, at least locally, a ca. 350 km depth (Artemieva and Mooney, 2001). Surface heat flow measured in numerous boreholes does not exceed 25–30 mW/m^2 over large interior parts of the Craton (Artemieva and Mooney, 2001). The results of thermal modeling are supported by the P–T arrays from mantle xenoliths, which indicate extremely cold (33–36 mW/m^2) reference geotherms for many kimberlite fields of the Anabar, Aldan and Alakit terranes (Fig. 1b) (Ashchepkov et al., 2010, 2013).

Interpretations of the seismic refraction ultra-long Soviet PNE (Peaceful Nuclear Explosions) profiles (which provide seismic velocity structure down to ca. 700 km) show that the upper mantle of the Siberian Craton is strongly heterogeneous, with the presence of a series of thin high-velocity and low-velocity layers beneath some parts of Siberia (Fuchs and Wenzel, 1997). Velocity anomalies associated with these multiple LVZs may sometimes be interpreted as the LAB (Priestley et al., 1994), although many profiles do not show any velocity change at ca. 200–250 km depth (Egorkin et al., 1987; Suvorov et al., 2010). For example, in agreement with regional heat flow and xenolith-constrained thermal models (which suggest the presence of, at least locally, deep lithospheric keels), the PNE profiles Craton, Kimberlite, Rift and Meteorite do not show the presence of any LVZs beneath the interior Siberian Craton down to the transition zone (Pavlenkova and Pavlenkova, 2006). Thermo-petrological interpretations of seismic Vp-velocity model along the PNE profiles Kimberlites and Meteorite indicate a 300 ± 30 km thick lithospheric mantle in the central part of the Craton (Kuskov et al., 2014) with a heterogeneous structure.

In contrast, large-scale (global or continent-scale) seismic tomography models suggest that lithosphere thickness beneath the Siberian Craton is ca. 250 km only (e.g. Priestley and Debayle, 2003; Priestly and McKenzie, 2006; Kustowski et al., 2008), although recent high-resolution tomographic models show a somewhat thicker LAB (ca. 250–300 km) (Schaeffer and Lebedev, 2013a). The discrepancy in the lithosphere thickness based on the PNE seismic profiles, thermal models and xenolith data, on one hand, and seismic tomography

* Corresponding author at: Oester Voldgade 10, Copenhagen, Denmark, 1350. Tel.: +45 440 793 101 2649.
E-mail address: yc@ign.ku.dk (Y. Cherepanova).

http://dx.doi.org/10.1016/j.gr.2014.10.002
1342-937X/

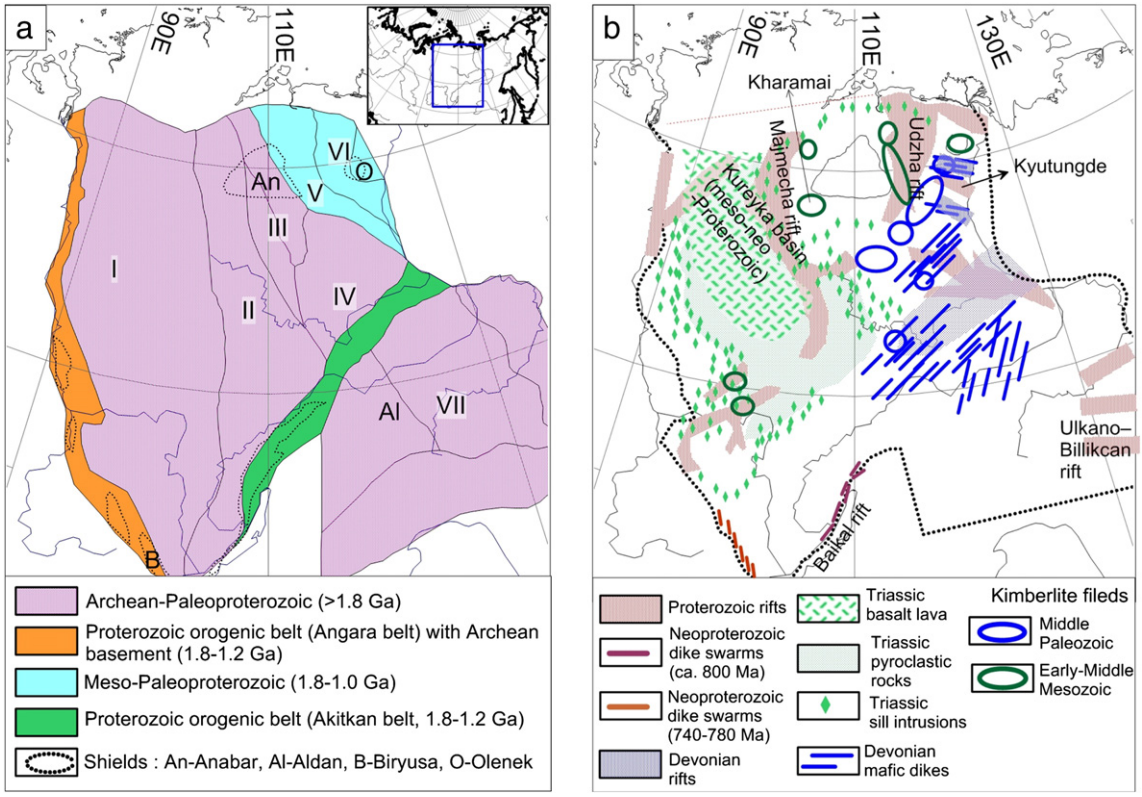

Fig. 1. Simplified tectonic map of the Siberian Craton (insert map in (a) shows location of the Craton). (a) Basement structure and (b) major magmatic and rifting events of the Siberian Craton (sources: Milanovsky, 1996; Kuznetsov, 1997; Reichow et al., 2002; Rosen, 2003; Gladkochub et al., 2007). (a) Thin black lines — boundaries between basement terranes; I–VI — Anabar subcraton with Archean terranes (I — Tunguska, II — Magan, III — Daldyn, IV — Markha terranes) and Proterozoic Olenek superterrane (V — Hapchan; VI — Birekte terranes); VII — Aldan–Stanovoy subcraton. (b) Bold dotted line — outline of the Siberian Craton. For color figure, please refer to the web version.

models, on the other hand, may (at least in part) be caused by low ray path coverage of the Craton (e.g. Kustowski et al., 2008; Schaeffer and Lebedev, 2013b) which hampers resolution of (possibly localized) deep lithospheric root(s).

Petrological, seismic, gravity and geothermal data indicate the existence of lateral and vertical heterogeneities in the lithospheric mantle of the Siberian Craton. Petrological studies of the Siberian mantle (based on mantle-derived xenoliths, garnet xenocrysts, garnets from heavy minerals concentrates and alluvial deposits) are spatially limited by known kimberlite fields (e.g. Pokhilenko et al., 1993; Boyd et al., 1997; Griffin et al., 1999b, 2005; Ashchepkov et al., 2010; Ionov et al., 2010). They indicate that the Siberian cratonic mantle is formed by highly depleted peridotites with a large amount of orthopyroxene as compared to off-cratonic mantle (Boyd, 1997). The wide-spread presence of eclogites in the Siberian mantle has been documented for several regions (Sobolev et al., 1994; Beard et al., 1996; Snyder et al., 1997; Pernet-Fisher et al., 2014).

A composite geochemical profile across the north-eastern part of the Siberian Craton based on petrological data (garnet concentrates) from major kimberlite fields shows a strong heterogeneity of the lithospheric mantle, with significant compositional variations over distances less than 50 km (Griffin et al., 1999b). It shows a decrease in orthopyroxene amount towards the Proterozoic terranes and rifted regions and an increase in harzburgitic composition beneath the Daldyn–Alakit kimberlite field. The vertical profile of the average Mg-number (Mg# = MgO/[MgO + FeO]) in the Siberian lithospheric mantle calculated from garnet compositions and bulk studies of mantle xenoliths shows a significant decrease of Mg# below a ca. 180 km depth (Agashev et al., 2013). In agreement with geophysical studies (Artemieva, 2009; Kuskov et al., 2014), it indicates a significant refertilization of the lithospheric mantle at depths greater than 180 km.

Separation of thermal and compositional anomalies in seismic tomography models shows that in the cratonic regions sampled by kimberlite magmatism the base of chemical boundary layer (CBL) is usually more shallow than seismic and thermal LAB (Artemieva, 2009). This led to the conclusion that kimberlite magmatism follows the lithosphere weakness zones and composition of the lithospheric mantle derived from xenoliths should not be representative of the pristine cratonic mantle (Artemieva, 2009, 2011). Reduced depletion in the basal part of the lithospheric mantle is interpreted to result from melt-related metasomatism. Infiltrations of melts caused by various tectono-magmatic events during a long geodynamic evolution of the cratons may locally refertilize cratonic mantle and produce bulk composition typical of younger SCLM or even similar to 'pyrolite' composition (Griffin et al., 2005; Artemieva, 2009). Given that large Precambrian cratons contain terranes of different ages that have been differently modified during their long history, one would expect to find significant lateral heterogeneity of the SCLM of the cratonic regions, including significant regional variations in mantle density.

Existing estimates of bulk density of subcontinental lithospheric mantle (SCLM) in South Africa (Jordan, 1979) and globally for lithosphere of different ages (Gaul et al., 2000; Poudjom Djomani et al., 2001) are based on average mineral composition of cratonic mantle (constrained by mantle-derived peridotite xenoliths and garnet–xenocryst suites) and experimental data on densities of the mineral end-members. These studies indicate that high buoyancy of the Archean SCLM relative to the asthenosphere results from its depleted composition and that lithosphere depletion progressively decreases (and its bulk density increases) from Archean through Proterozoic to Phanerozoic age. These correlations between lithosphere age and composition (and hence density) are constrained from xenoliths and xenocrysts from kimberlites and thus are limited by the areas of kimberlite pipes.

On a regional scale, density structure of the upper mantle in Siberia has been studied primarily by gravity modeling (Artemjev et al., 1994; Kaban et al., 2003), although some attempts have been done to convert

P-wave velocities along some of the PNE seismic profiles to densities (Romanyuk, 1995; Kuskov et al., 2014; Yegorova and Pavlenkova, 2014). However, given a large uncertainty in the correlation between seismic velocities and densities (Barton, 1986) and different sensitivity of velocities and densities to variations in mantle composition (c.f. Artemieva, 2011), the results based on such an approach are questionable. Global-scale gravity modeling for SCLM (Kaban et al., 2003) indicates that the Siberian Craton is one of the areas with the largest positive mantle residual gravity anomalies (calculated by the removal of crustal gravity effect from the Bouguer gravity anomalies) and the most significant negative residual topography, which indicate a very low density of the SCLM. However, this and other regional gravity models (Artemjev et al., 1994) have low spatial resolution, due to restrictions on land-gravity data and the absence at that time of a high resolution regional crustal model. As a result, they could not resolve regional variations in mantle density and thus cannot be directly compared to the peridotite xenoliths dataset.

The availability of satellite gravity data and a new detailed seismic crustal model for Siberia (Cherepanova et al., 2013) opens new possibilities for regional gravity modeling (Herceg et al., submitted for publication). Limited number of studies of mantle density of the Siberian Craton and an importance of this information for understanding structure and preservation of thick cratonic keels has motivated our study. The approach is based on free-board buoyancy modeling (Lachenbruch and Morgan, 1990) and is justified by near-zero free-air gravity anomalies over most of the region, which indicate its nearly complete isostatic equilibrium. In our analysis, we take an advantage of a new high quality regional seismic crustal model (Cherepanova et al, 2013), high resolution digital topography model ETOPO1 (Amante and Eakins, 2009), and regional thermal model (updated after Artemieva, 2006). These datasets allow us to analyze relative contributions of the crust and the subcrustal lithosphere in maintaining surface topography and thus to model mantle density structure, both at in situ and at room (SPT, standard pressure–temperature) conditions. The former provides a possibility to compare mantle densities with seismic velocities and to test the isopycnic condition for the Siberian mantle, while the latter — to compare the results with xenolith data.

2. Geological setting

2.1. Precambrian tectonics

The basement of the Siberian Craton is formed by the assemblage of Archean and Proterozoic terranes (Rosen et al, 1994; Rosen, 2003; Gladkochub et al., 2006) (Fig. 1a). The collision (at 2.0–1.9 Ga) between the Aldan and the Anabar blocks, possibly related to the assembly of a Paleoproterozoic protocontinent (Meert, 2002; Rogers and Santosh, 2002; Zhao et al., 2002), completed the formation of the Craton and produced juvenile Paleoproterozoic crust along the Akitkan magmatic-fold belt which makes a major intracratonic suture zone (Zonenshain et al., 1990; Condie and Rosen, 1994).

The Archean and Paleoproterozoic basement rocks are exposed and dated in few areas only: (i) the Anabar Shield in the north-central part; (ii) the Olenek High in the north-eastern part; (iii) the Yenisey Ridge in the west; (iv) two areas in the Biryusa block in the south-west; (v) the Aldan Shield and the Stanovoy block in the south-east. The boundaries between the terranes are defined entirely from geophysical data (Rosen et al., 1994; Rosen et.al.,2000) as most of the Craton is covered by a several km thick layer of Riphean–Phanerozoic sediments (Cherepanova et al., 2013), including the Permo-Triassic flood basalts which fill the Tunguska Basin (Reichow et al., 2009) (Fig. 1b).

2.2. Rifting and basin subsidence

In Proterozoic, the Siberian Craton was rifted along the southern margins, while extensional events formed a series of intracratonic sedimentary basins (Fig. 1b). The oldest rifts were formed at ~1.73–1.68 Ga at the south-eastern margin of the Aldan Shield (the Ulkano–Billikcan Rift) and at the south-western part of the Biryusa block (Gladkochub et al., 2007). Mesoproterozoic rifting formed the Udzha and Majmecha rifts along the eastern and western margins of the Anabar Shield (Milanovsky, 1996) and caused a rapid post-rifting subsidence of the Craton at around 1.6 Ga (Zonenshain et al., 1990). Overall, the Proterozoic rifting, possibly associated with the break-up of Rodinia, led to the formation of ca. 1–4 km deep intracratonic basins and 10–14 km deep basins along the cratonic margins (Pisarevsky and Natapov, 2003; Cherepanova et al., 2013); the latter are interpreted to have been formed at passive continental margins (Sklyarov et al., 2001). Only few areas did not experience the Proterozoic subsidence: the Aldan–Stanovoy and Anabar Shields, the Nepa–Botuoba block, and some small areas in the western and north-eastern parts of the Craton.

A large-scale Devonian thermal event (possibly related to a mantle plume) significantly affected the SE part of the Craton and formed (or reactivated) the long and wide Viluy Rift system (Fig. 1b). It roughly follows the Paleoproterozoic Akitkan orogenic belt and extends sublatitudinally over 600 km across the Craton interior and plunges under the Verkhoyansk fold belt. The rifting was accompanied by substantial mafic and kimberlite magmatism (Parfenov and Kuz'min, 2001; Courtillot et al., 2010) and was followed by a significant post-rifting subsidence with the accumulation of 7–8 km of Devonian–Lower Carboniferous sediments within the 12–14 km deep Viluy Basin. In the Early–Middle Carboniferous, the Tunguska Basin became a major subsidence area of the Craton with accumulation of 8 km of sediments, but rifting as the cause of basin subsidence has not been proven. The Devonian rifting formed the Kyutungda Rift at the north-eastern margin of the Craton; the consequent Early-Carboniferous rifting has further affected the Olenek block in the north-eastern part of the Craton.

2.3. Intraplate magmatism

The major phases of volcanic activity within the Siberian Craton include (i) a widespread Neoproterozoic (780–740 Ma by ^{40}Ar–^{39}Ar dating) mafic dike volcanism over the southeastern and southern parts of the Craton, possibly related to the break-up of Rodinia (Gladkochub et al., 2006), (ii) several pulses of Phanerozoic kimberlite volcanism (420–380 Ma, 380–340 Ma, 245–240 Ma, and 170–140 Ma; no Riphean kimberlite pipes are known), and (iii) the Permo-Triassic trap-basalt volcanism (Fig. 1b).

The Devonian rifting of the Viluy Basin was accompanied by the wide spread of mafic dikes. All of the Upper Devonian–Lower Carboniferous kimberlites lie in the region between the Anabar Shield and the Vilyui Rift, and form a nearly linear belt parallel to the strike of the Viluy Rift. Major kimberlite fields (the Daldyn–Alakit, the Malo–Botuoba, the Upper Muna, and several others) were formed by the wide-spread Late Paleozoic (380–240 Ma) magmatism along major pre-existing lithospheric sutures (Davis et al., 1980; Ilupin et al., 1990). The Lower Triassic kimberlitic magmatism (245–240 Ma) took place along the eastern margin of the Anabar Shield and locally at its western side within the Majmecha Rift. The last pulse (170–140 Ma) of kimberlite eruptions, which affected the western part of the Anabar Shield and the north-eastern part of the Siberian Craton, may have followed the pre-existing Majmecha Rift and the Devonian rift along the eastern part of the Olenek terrane, correspondingly (Milanovsky, 1996).

The major Permo-Triassic magmatic event is the Siberian flood basalt magmatism. The basalts, tuffs and near-surface intrusive rocks cover approximately 40% of the Siberian Craton with an average lava thickness of ~3.5 km (locally >6 km) in the Tunguska Basin (e.g. Wooden et al., 1993; Fedorenko et al., 1996) and thinning to a few tens of meters towards the southeast (Vyssotskiy et al., 2006). The presence of the belt of Lower Triassic (younger than the Siberian traps) alkali-ultramafic intrusions with carbonatites to the west of the

Anabar Shield suggests some extensional tectonics, although there is no evidence for a Triassic rifting of the Craton.

3. Free-board buoyancy modeling

3.1. Method and model assumptions

Surface topography (Fig. 2a) is controlled by thickness, composition, metamorphic state, and temperature of the crust and lithospheric mantle, and dynamic contribution from the mantle (Artemieva, 2007). Near-zero (in the range ±30 mGal, locally down to −60 mGal) free-air gravity anomalies (Herceg et al., submitted for publication) suggest that the region is in the isostatic equilibrium and thus the effect of dynamic topography is insignificant for most of the Craton (Fig. 2b). Local positive anomalies (up to +30 mGal) are observed beneath the Anabar Shield, the northern part of the Putorana Plateau and the Aldan terrane. The strongest negative anomalies (−30 mGal, locally −60 mGal) follow the Akitkan belt from the Viluy Basin towards the Baikal, where they form a narrow belt located beneath the Baikal Rift Zone.

In the absence of dynamic topography, surface topography is the sum of the isostatic contributions of the crust and lithospheric mantle (see Appendix A for details). Mantle density may be modeled by free-board (buoyancy) mass balance calculations (Lachenbruch and Morgan, 1990; Artemieva, 2003, 2007), which are based on the following assumptions:

(i) the isostatic balance is achieved at the base of the lithosphere; the validity of this assumption is supported by the near-zero free-air gravity. Although the compensation depth is unknown, in the absence of dynamic support from the mantle it should not be deeper than the lithosphere–asthenosphere boundary (LAB);

(ii) flexural rigidity of the lithosphere is ignored, i.e. it is assumed that individual lithospheric blocks can move independently as piano keys. This assumption is difficult to validate but it is partially supported by study of flexural rigidity of the lithosphere of the Siberian Craton (Poudjom Djomani et al., 2003), which indicates unusually low Te values (ca. 10–16 km in the kimberlite provinces increasing to ca. 40 km in adjacent regions). These low values typical of tectonically young regions rather than a craton suggest that the cratonic lithosphere may be disrupted into a series of individual blocks which thus cannot support flexural rigidity of the Craton;

(iii) pressure-dependence of density is neglected; the validity of this assumption in the absence of phase transitions and near-zero rock porosity is supported by theoretical models and laboratory data (Semprich et al., 2010; Yang et al., 2014);

(iv) density of sublithospheric mantle (asthenosphere) is constant. We have adopted its value of 3.235 t/m^3 (1 t/m^3 = 1 g/cm^3 = 1000 kg/m^3) at in situ mantle conditions (T = 1300 °C), which corresponds to density of 3.39 t/m^3 at room (SPT) conditions (Anderson, 1987; Irifune, 1987), assuming thermal expansion coefficient of 3.5×10^{-5} 1 / K.

Calculations of the isostatic contributions of the crust and lithospheric mantle require data on the surface topography, the thicknesses and density structure of the crust and the lithospheric mantle, and the lithospheric geotherms (the Moho temperatures) (Fig. A1). We next discuss our choice of the model parameters and perform sensitivity tests to examine the effect of the parameter choice on the modeling results.

3.2. Input parameters

3.2.1. Topography

Surface topography is constrained from the ETOPO1 digital 1 arc-minute global relief database (Amante and Eakins, 2009). These high resolution data are interpolated on a 1° × 1° regular grid to achieve the same spatial resolution as other model parameters (thermal and crustal models). A long-lasting tectonic development of the Siberian Craton as a stable platform has leveled its surface topography to an

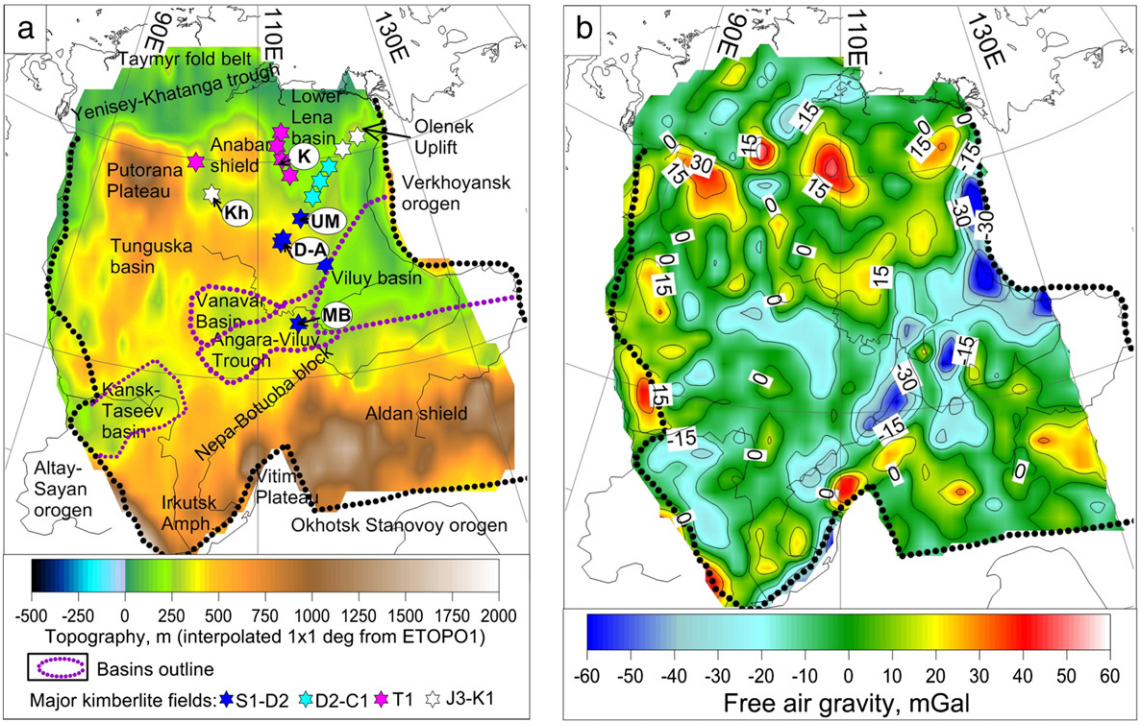

Fig. 2. (a) Topography based on ETOPO1 (Amante and Eakins, 2009) and (b) free air gravity anomaly based on GOCE satellite data (Pail et al., 2011). Dotted lines in (a) — outlines of major intracratonic basins. Stars — major kimberlite fields. Abbreviations: S1–D2 = 420–380 Ma, D2–C1 = 380–340 Ma, T1 = 245–240 Ma, J2–K1 = 170–140 Ma. Kimberlite fields discussed in the paper: Malo–Botuoba (MB), Daldyn–Alakit (D–A), Kharamai (Kh), Kuonamka (K), Upper Muna (UM). For color figure, please refer to the web version.

average elevation of ca. 400 m above sea level with regional undulations within a 200–300 m range over much of the Craton interior (Fig. 2a). Most prominent regional uplifts include the Anabar Shield where the elevation reaches 700 m and the volcanic Putorana Plateau in the northwest of the Craton with local highs up to 1250 m. The Aldan–Stanovoy mountain region, which forms a major cratonic terrane in the southeast, is uplifted to 700–1300 m a.s.l., with the highest elevation around the volcanic Vitim Plateau at the eastern terminus of the Baikal Rift Zone. The lowest topography is typical of the intracratonic rifted basins, including the Viluy Basin (200–275 m a.s.l.), the Angara–Viluy Trough in the central part of the Craton, and the Kansk–Taseev Basin in the west, with the lowest topography (100–200 m a.s.l.) recorded in the Lower Lena Basin to the east of the Anabar Shield.

Topography at the cratonic margins is highly variable and ranges from depressions of the Yenisey–Khatanga–Lena Troughs to the north of the Craton, to low-lands of the West Siberian Basin in the west, to Alpine collisional belt of the Verkhoyansk Mountains in the east, and the Altay–Sayans Mountains in the south-west. Regions with a high mountainous topography show strong free-air anomalies. Given that isostatic balance is an important assumption in the present modeling, we have excluded these regions from the analysis, while the density structure of the upper mantle beneath the West Siberian Basin is a subject of a separate study (Cherepanova and Artemieva, subm.).

3.2.2. Crustal structure and the Moho depth

Crustal structure of the region is well constrained by a new high quality regional crustal model SibCrust, which is based on compilation of all available crustal-scale seismic profiles for Siberia and excludes any gravity constraints (Cherepanova et al., 2013). The SibCrust model is specified by 12 parameters which include thickness and Vp velocity of 5 crustal layers (sediments, upper, middle, lower, and fast lowermost crust), the Moho depth, and the sub-Moho Pn velocity. The model is constrained along seismic profiles, which were digitized with a lateral spacing of not more than 50 km; however, in some parts of the region the spacing between the adjacent profiles may reach up to ca. 250 km. To have a uniform coverage of the region by a crustal model, for each of the model parameters the SibCrust model constrained along seismic profiles has been interpolated with a 300 km search radius, chosen to close data gaps, and saved on a $1^\circ \times 1^\circ$ grid, which corresponds to the spatial resolution of the thermal model.

The crustal structure is well correlated with the tectonic elements of the Craton (Fig. 3b). Thick (43–46 km) crust with a three-layer structure typical for Precambrian platforms dominates most of the Craton interior. Crustal roots down to a 50 km depth are present in the Aldan–Stanovoy terrane, but information on the crustal structure of this part of the Craton is limited to one sublatitudinal profile (for seismic data coverage and the discussion of SibCrust resolution see Cherepanova et al., 2013). The crust is thinned to ca. 40 km in the intracratonic basins, with the smallest thickness (ca. 36–38 km) in the central part of the Viluy Basin. Thickness of sediments varies from near-zero in the Anabar and Aldan Shields to ca. 3–5 km over most of the Tunguska Basin, to ca. 1–3 km at around the major kimberlite fields in the Daldyn–Alakit province, and to 12–14 km in the Viluy Basin and in the Lena foredeep along the eastern margin of the Craton.

Mass balance calculation requires knowledge on density structure of the crust. First, for each crustal layer Vp velocities were converted to densities, using the mid-point line between published conversion velocity–density relationships as constrained by laboratory studies on crustal rocks (Ludwig et al., 1970; Henkel, 1994; Christensen and Mooney, 1995). The exception has been made for the sedimentary layer, where the velocity–density conversion was chosen to correspond to maximum, but not mean, densities. This choice is governed by regional structure of the sedimentary cover which includes high-density metasediments over all of the Craton interior. Due to compaction, high-density sedimentary fill is also expected in the ca. 12–14 km deep Paleozoic Viluy Basin. Finally, the average in situ density of the entire crust was calculated as weighted average with account for thickness of individual crustal layers (Fig. 3a).

Crustal density structure is highly heterogeneous with significant variations (from ca. 2.75 to ca. 2.88 t/m^3), which are only weakly correlated with the Moho depth. On the whole, we do not observe any systematic relation between the basement age and the average crustal density. The latter is clearly controlled by tectonic setting and geodynamic evolution, although the Archean crust of Siberia apparently has higher average density than Proterozoic crust. The highest bulk crustal density (2.84–2.88 t/m^3), in part due to the presence of a thick (18–20 km) lower crustal layer, is typical of the Anabar and Aldan Shields, where sedimentary cover is nearly-absent. Similar values are typical of the Olenek basement high in the north-east. Low crustal density is characteristic of the Akitkan belt and deep rifted basins, which are well expressed in crustal density structure.

3.2.3. Lithosphere geotherms and LAB depth

Our modeling is based on the assumption that the isostatic balance is achieved at the base of the lithosphere (LAB), and thus knowledge on the lithosphere thickness is crucial. The isostatic contributions of both the crust and the lithospheric mantle also depend on their temperatures, so for consistency of our calculations we define the base of the lithosphere (LAB) as the base of the thermal boundary layer (TBL), defined locally by the intersection of conductive geotherm and mantle adiabat with temperature of 1300 °C. Thus knowledge of lithosphere geotherms provides both, the lithosphere thickness and the Moho temperature. The latter is used to calculate average temperature of the SCLM, defined as mid-temperature between temperature at the Moho (locally variable) and the LAB (fixed at 1300 °C). Density structure of the crust is constrained by seismic velocities and thus refers to in situ conditions. For this reason, we perform the analysis of the SCLM density also at in situ temperatures, and then recalculate it to room temperature to compare our modeling results with xenolith data.

The thermal structure of the lithosphere is based on the analysis of regional heat flow data measured in a large number of 500 m to 3000 m deep boreholes (Artemieva and Mooney, 2001). Most of the boreholes are located in the south-western part of the Craton, along the Akitkan belt, in the major kimberlite provinces of Daldyn–Alakit and Malo–Botuoba, the western part of the Aldan terrane, and in the Viluy Basin and its vicinity. Some isolated heat flow measurements are reported for the Tunguska Basin, the Anabar Shield, and the central part of the Aldan terrane (here the boreholes are 100–500 m deep); however no heat flow data are available for significant parts of the Magan, Hapchan, Birekte, and Aldan terranes. To cover the data gaps, the thermal model based on regional heat flow measurements (Artemieva and Mooney, 2001) has been supplemented by statistical values of lithospheric geotherms for terranes with similar basement ages and tectonic evolution, further calibrated by world-wide data on xenolith P–T arrays (Artemieva, 2006) (Fig. 3c).

The resultant model of the lithosphere thermal thickness is shown in Fig. 3d. Thick (300–350 km) lithosphere forms a sublongitudinal belt in the central part of the Craton where extremely low heat flow values (18–25 mW/m^2) are measured over a large territory from the Anabar Shield in the north, across the Daldyn–Alakit and Malo–Botuoba kimberlite provinces, and to the Irkutsk Amphitheater in the south, where heat flow increases to 32–38 mW/m^2. Very low surface heat flow (22–28 mW/m^2) is also reported for deep boreholes in the Angara–Yenisey belt along the western cratonic margin. Very low heat flow implies an extremely low lithospheric geotherm and a thick lithosphere, even when assuming a very low crustal heat production (ca. 0.4 μW/m^3 typical of granulite terranes). In these regions the exact thickness of the TBL is difficult to determine, since at depths greater than 300 km conductive geotherm asymptotically approaches mantle adiabat (Artemieva and Mooney, 2001).

In our model we have adopted the value of 350 km as the maximum thickness of the TBL. This value is in agreement with xenolith P–T arrays

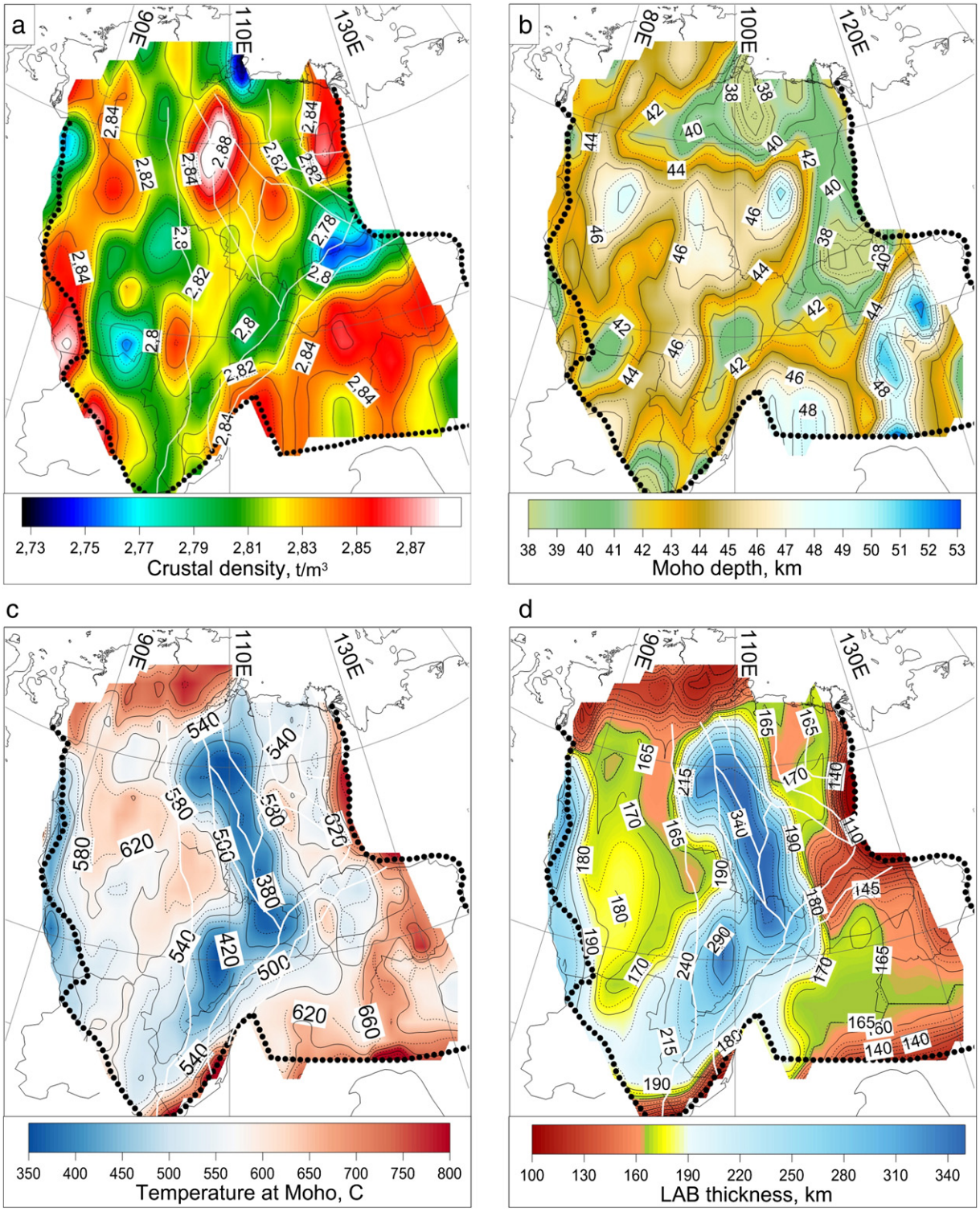

Fig. 3. Input parameters for free-board modeling: crustal and lithosphere structure of the Siberian Craton. (a) Average crustal density (including sediments); (b) the Moho topography; (c) temperature at the base of the crust; (d) lithosphere thermal thickness. Data sources: (a) and (b) based on the SibCrust model (Cherepanova et al, 2013); (c) and (d) — on the TC1 thermal model (Artemieva, 2006). White thin lines indicate the major suture zones of the basement (see Fig. 1a for details). Density units: 1 t/m^3 = 1 g/cm^3 = 1000 kg/m^3. For color figure, please refer to the web version.

for the kimberlite fields of the Anabar, Aldan and Alakit terranes, which indicate extremely cold (33–36 mW/m^2) reference geotherms (Ashchepkov et al., 2010, 2013) that imply the TBL thickness of at least 300–350 km (Pollack et al., 1993). Similarly, the present-day geotherms beneath the Siberian Craton, calculated from Vp-velocities along two long-range PNE Soviet seismic profiles, and with account for petrological data for peridotite xenoliths, fall close to 32.5–35 mW/m^2 conductive geotherms and indicate the presence of, at least, 300 km thick lithospheric keel (Kuskov et al., 2014).

3.2.4. Density structure of the SCLM

Similar to gravity modeling, the free-board modeling can constrain only average density of the SCLM, which is integrated vertically over its entire depth. It means that the depth distribution of density

variations within the lithospheric mantle may have any pattern. For the sake of simplicity and in the absence of other data, we assume that, for any $1^\circ \times 1^\circ$ cell, the density structure of the SCLM is homogeneous through the entire chemical boundary layer, CBL. In our analysis, we examine two models for the CBL thickness. For both models, the calculations are based on the same crustal and thermal models as described above.

One-layer Model 1 (Fig. 4a) is based on the assumption that the bases of the thermal and chemical boundary layers (TBL and CBL) are at the same depth. This model provides the density value for the SCLM integrated over the depth from the Moho to the LAB.

World-wide and regional xenolith data indicate vertical stratification of cratonic lithospheric mantle with a high Mg# in the upper layer (from the Moho down to ca. 180 km depth) and a fast decrease of Mg# to an essentially fertile composition below a 180 km depth (Fig. 6.15 in Artemieva, 2011). Such a pattern with a fast drop of Mg# in olivine at a 180 ± 20 km depth is well recognized for the Siberian kimberlite provinces (Griffin et al., 1999a, 2005). We use this petrological data as the basis for our Model 2.

Two-layer Model 2 (Fig. 4b) assumes a two-layer compositional stratification of the lithospheric mantle, as reported for some parts of the Slave Craton and the Baltic Shield (Kopylova and McCammon, 2003; O'Brien et al., 2003). In this model, we assume that the CBL extends from the Moho down to 180 km depth (and thus, on average the CBL is ca. 135–140 km thick). Below this depth and down to the LAB, the composition of the lithospheric mantle is assumed to be close to fertile, but still slightly depleted as compared to pyrolite (primitive) mantle. The latter is assumed to have SPT density of 3.39 t/m^3 (equivalent to in situ 3.235 t/m^3).

The choice of the density value for the bottom SCLM layer is constrained by petrological data from Siberia. Bulk rock studies of deep, high-T peridotites from the Udachnaya pipe (Agashev et al., 2013) indicate that the average bulk Mg# of the deep SCLM layer is ca. 89.5. Similar values for Mg# in olivine are reported in studies of garnet concentrates from peridotites brought from depths of 180 km and deeper (Griffin et al., 2005). Mg# = 89.5 corresponds to average mantle density of 3.38 t/m^3, when calculated from the isopycnic correlation (Jordan, 1988). The latter value is adopted here as SPT density of the deep SCLM layer in Model 2 (Fig. S1b). This value is ca. 0.02–0.04 t/m^3 higher than the average SPT density calculated in Model 1 for the parts of the Siberian Craton where the lithosphere extends deeper than 180 km depth (Fig. S4a).

We find it possible that isopycnicity (if satisfied for the Siberian Craton, in general, and for the region with the deep LAB, in particular) may be achieved for the lithospheric column on the whole but not necessarily at any depth between the Moho and the LAB (Kelly et al., 2003). Due to low lithospheric temperatures in the bottom (up to 170 km thick) SCLM layer in those parts of the Craton where the lithospheric root is extremely thick (Fig. 3d), fixing SPT density of the bottom layer in Model 2 at 3.38 t/m^3 leads to a regionally high (3.24–3.26 t/m^3) in situ density of this layer (Fig. S1b). These values exceed the assumed in situ density of the pyrolitic mantle (3.235 t/m^3), and at SPT conditions correspond to the extreme values of 3.41–3.49 t/m^3 in the bottom layer in Model 2 which may be expected for mantle enriched in the garnet and eclogitic modes.

3.2.5. Isostatic height of sea level

The calculation scheme includes a free parameter D, the constant which is the isostatic height of sea level above the asthenosphere (Figs. A1, S2). This constant is the easiest to calculate at mid-ocean ridges, given that there the base of the lithosphere coincides with the Moho. A commonly used value of D = 3.5 km is calculated assuming the Moho depth of 5.5 km, the water depth of 3.5 km, and the average crustal density of 2.8 t/m^3 (Lachenbruch and Morgan, 1990). Although the chosen values correspond to typical observations over mid-ocean ridges, they do not guarantee that regions with these parameters of crustal structure and bathymetry are in isostatic equilibrium as required by the nature of the free parameter.

Thus, as the first step in our modeling, we have re-evaluated the constant D by choosing the segment of the mid-ocean ridge where free air

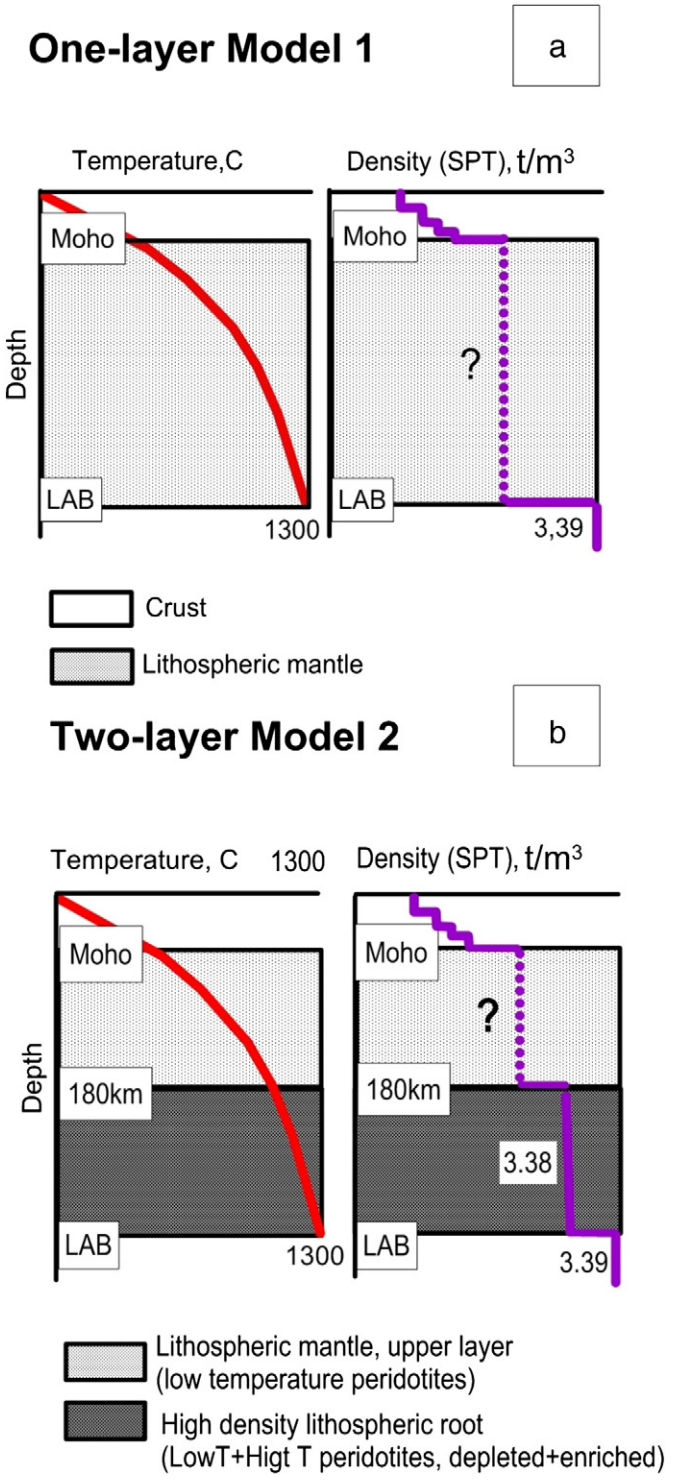

Fig. 4. Two models of the chemical boundary layer used in free-board calculations. Top: one-layer Model 1 (after Lachenbruch and Morgan, 1990). The unknown lithospheric mantle density is the average density between the Moho and the LAB. Bottom: two-layer Model 2, which assumes the presence of a nearly-fertile layer below a 180 km depth down to the LAB with a fixed SPT density of 3.38 t/m^3. The chemical boundary layer with unknown density is between the Moho and 180 km depth. Thermal structure, the Moho depth and the lithosphere thickness in Models 1 and 2 are the same. See text and Fig. A1 for explanation.

anomaly is near-zero (Fig. S2a). Surprisingly, the area around the triple junction of the Pacific, Nazca and Cocos plates (around 0.5 S–1.5 S) with the highest spreading rates is basically the only part of the global mid-ocean ridge system which is isostatically compensated, with the free air gravity anomaly of ±5 mGal (Herceg, personal comm.). In this area, the water depth above the mid-ocean ridge is ca. 2.9–3.0 km in the area with the near-zero free air gravity anomalies (Fig. S2b).

Fortunately, there is a seismic profile which crosses the ridge at ca. 1.9 N; it indicates the Moho depth of ca. 5–6 km (Zonenshain et al., 1980). Given the uncertainty in the Moho depth and the average crustal density, we calculated a family of possible solutions for the constant D (Fig. S2c) by varying crustal density, the Moho depth, and the bathymetry.

For further modeling we have adopted the value of D = 4.25 km which, in agreement with data for the chosen segment of the Pacific ocean, corresponds, for example, to a 6 km thick crust with 2.75 t/m^3 density and 3 km bathymetry. Our analysis illustrates that for the reported values of the crustal thickness and bathymetry observed in this oceanic segment, the value of D = 3.5 km (Lachenbruch and Morgan, 1990) requires unrealistically high crustal density (>2.9 t/m^3). The effect of the choice of the constant D on the modeling results is examined in the sensitivity tests (Table 1), together with the effects of uncertainties in other parameters.

3.3. Sensitivity tests

We run a set of sensitivity tests to examine how uncertainties in the model parameters propagate to uncertainty in the final density model of the SCLM (Table 1). Major uncertainties are associated with the crustal model, thermal model, and the choices of the constant D and the asthenosphere density. To test the sensitivity of the results, all parameters, except for the one in question, are fixed at the values described in Table 1 (reference model), and only the parameter in question is modified to the maximum value of its expected uncertainty. We next provide some comments to the choice of the tested parameters.

True uncertainties in the crustal model are difficult to estimate, since significant discrepancies exist even in the Moho depth reported by different authors for the same parts of the region (Cherepanova et al., 2013). These discrepancies exceed the uncertainty of seismic methods used in crustal studies, and thus error bars for the resultant model cannot be estimated. A comparison of the SibCrust model with global crustal models CRUST1.0 and CRUST2.0 (Bassin et al., 2000; Laske et al., 2013) for Siberia also shows significant discrepancies in all parameters that specify the crustal structure. We thus ran sensitivity tests with common discrepancy values for the Moho depth and the average crustal P-wave velocity. Since crustal density is constrained from Vp, the test for crustal density variations also inexplicitly incorporates the uncertainty in the velocity–density conversion (e.g. Barton, 1986).

In our definition of the LAB (as the base of the TBL), testing variations in lithosphere thickness also means testing the effect of the thermal model uncertainty on the final results. The base of the thermal lithosphere constrained by heat flow data (Artemieva and Mooney, 2001) and xenolith P–T arrays (Ashchepkov et al., 2010) is resolved with an uncertainty of 25–50 km, which is ca. 15–25% for the entire range of the LAB depth values greater than 100 km. As mentioned above, there is a large discrepancy in the LAB estimates for Siberia between thermal models, xenolith P–T arrays, and the Soviet PNE profiles, on one hand, and large-scale seismic tomography models (Levshin et al., 2001; Villaseñor et al., 2001; Pasyanos, 2010), on the other hand. Furthermore, a recent seismic tomography model can resolve the presence of >+3 + 4% Vs anomaly at 260 ± 30 km depth beneath the central part of the Craton (Schaeffer and Lebedev, 2013a). It is outside the scope of this study to address the nature of the discrepancy in the LAB estimates for the Siberian Craton. We note, however, that the lack of seismic stations and events in Siberia (Schaeffer and Lebedev, 2013b) results in a poorly resolved upper mantle structure of the Craton. The ambiguity in amplitudes of resolved seismic velocity anomalies associated with the choice of reference models (Priestley and Debayle, 2003) and damping procedure in tomography inversions (Legendre et al., 2012; Foulger et al., 2013), as well as the ambiguity in the choice of the velocity-anomaly value as the base of the lithosphere (Artemieva, 2009) hampers straightforward use of seismic tomography models to determine the LAB depth beneath Siberia. Nonetheless, we use the results of some regional tomography models to test how the density modeling results may change if, in the region with the lowest surface heat flow, we fix the LAB at 220 km depth (Fig. S3a), with the corresponding change in lithospheric temperatures (the coldest Moho temperatures increase to ca. 500 °C, compare with Fig. 4c). We find that in the region with the maximal imposed change in the LAB depth, the maximum change in the SCLM density is 0.014 t/m^3 (ca. 0.4%, Fig. S3d).

We test the effect of the free constant D on mantle density and examine correlation between the resultant density and the lithospheric thickness (Fig. S5). The choice of the D-value is most significant for the lithosphere that is less that 200 km thick, where the difference in density values calculated for D = 3.5 km and 4.25 km may reach 0.04 t/m^3. If the lithosphere is more than 200 km thick, the maximum observed density difference drops to 0.015 t/m^3 and it reduces to 0.008 t/m^3 for the lithosphere thicker than 270 km.

We expect that a typical uncertainty associated with any of the parameters is a half of the values presented in Table 1, where the tests are presented for the maximum values of expected uncertainties in the model parameters. Given that it is unlikely that, at any location, the errors in all model parameters will sum up, we estimate the overall uncertainty of the final density model as better than 0.02 t/m^3 or ca. 0.6% with respect to primitive mantle. Since petrological data indicate a 1.5–2.5% density anomaly in the Archean SCLM and 0.9–1.5% in the Proterozoic SCLM as compared to primitive mantle (Boyd and McCallister, 1976; Boyd, 1989; Hawkesworth et al., 1990; Griffin et al., 1998), the approach allows for a reliable distinction of lithospheric blocks with different tectonic evolution and their meaningful comparison with petrological data.

Table 1
Sensitivity tests.
Tests are presented for the maximum values of expected uncertainties in the model parameters.

Parameters	Reference model[a]	Parameter variation with respect to reference model	Change in SCLM density with respect to the reference model	
			t/m^3	%
Crustal density (SPT)	2.80 t/m^3	+0.05 t/m^3	0.02–0.03	0.6–0.8
Crustal thickness	44 km	+5 km	0.03	0.8
LAB thickness	165 km	+20%	0.01–0.02	0.3–0.6
Asthenosphere density (SPT)	3.39 t/m^3	+0.02 t/m^3	0.01–0.03	0.3–0.8
Constant D	4.25 km	0 to −0.75	0.02	0.06

[a] By reference model we mean here the average value of a parameter calculated for the entire study region. Density units 1 t/m^3 = 1 g/cm^3 = 1000 kg/m^3.

4. Results: density structure of the lithospheric mantle

Major result of our analysis is the density structure of the lithospheric mantle beneath the Siberian Craton and the adjacent areas. We present the results as four maps for lateral variations in the SCLM density: for one-layer Model 1 (Fig. 5a, b) and for two-layer Model 2 (Fig. 6a, b), and for both models the results are presented at in situ conditions (that is at P–T conditions that correspond to geophysical remote sensing, such as seismic modeling) and at SPT (standard P–T, i.e. room) conditions (that correspond to laboratory petrological studies of mantle-derived xenoliths). The results indicate the presence of a strong lateral mantle density heterogeneity beneath the entire Siberian Craton, well correlated with the tectonic setting.

4.1. Mantle density at SPT conditions

In cratonic lithosphere, the effects of thermal and compositional (due to depletion in basaltic components) heterogeneity on density tend to compensate each other (isopycnicity hypothesis, Jordan, 1975, 1988). To separate these competing effects and to extract mantle density anomalies caused by compositional heterogeneity alone, we recalculated in situ density anomalies to standard (laboratory) pressure–temperature, SPT, conditions since they allow for a direct comparison with petrological data. Calculations of SCLM density from average mineral compositions of mantle peridotites sampled by different magmatic processes suggest that density of the Archean mantle is ca. 3.31 ± 0.02 t/m^3, of the Proterozoic mantle ca. (3.34–3.35) ± 0.02 t/m^3, and of the Phanerozoic mantle ca. 3.36–3.39 t/m^3 (Griffin et al., 1999a; Poudjom Djomani et al., 2001).

We first focus our discussion on the results for one-layer Model 1 (Fig. 5b). For this model, the average SPT density of the lithospheric mantle is in the range from 3.31 t/m^3 to ca. 3.40 t/m^3 and covers the entire range of density calculated from average mineral compositions as constrained by mantle xenoliths (Griffin et al., 1999b; Poudjom Djomani et al., 2001).

The lowest (Archean) density values of 3.31–3.35 t/m^3 calculated for the Siberian mantle (Fig. 5b) correspond to density of the Kaapvaal peridotites. Values at the lower end of this range (3.31–3.33 t/m^3) were reported for low-T peridotites (Pearson et al., 1995), harzburgites and garnet lherzolites (Boyd, 1989). In the Siberian mantle, "Proterozoic" density values (3.34–3.35 t/m^3), similar to those calculated for all Kaapvaal peridotites (3.353 t/m^3, Jordan, 1979), are modeled for the central part of the Craton, in particular for the Proterozoic Akitkan belt, while high density values (3.38–3.40 t/m^3) are restricted to the rifted parts of the Craton (further discussed in Section 4.2).

Our two-layer Model 2 (Fig. 6a, b), as discussed in Section 3.2, is based on petrological studies of mantle xenoliths, which indicate that the lower part of the lithospheric keel may be refertilized during lithosphere–mantle interaction. For this model, the average density of the top layer of the lithospheric mantle is significantly lower than in Model 1, in particular in regions with deep lithospheric keels, where all density anomaly associated with SCLM depletion is "squeezed" into the upper layer with a thickness of ca. 135–140 km only. In regions with a low mantle density, the difference between Model 1 and the upper layer of Model 2 is up to 0.02 t/m^3 (at SPT) (Fig. S4a). The upper limit of the density values calculated in Model 2 does not change as compared to Model 1, because dense mantle is typical of regions with a less than 180 km thick lithosphere.

At SPT conditions, density of the upper SCLM layer is in the range from 3.29–3.30 t/m^3 to ca. 3.40 t/m^3 (Fig. 6a). Note that even the lowest density calculated for the Anabar Shield is close to the range of density values calculated for selected garnet peridotites, 3.305 t/m^3 (Hawkesworth et al., 1990), low-T Kaapvaal garnet peridotites, 3.30 t/m^3 (Boyd and McCallister, 1976), as well as to the values calculated for average mineral compositions of mantle peridotites from the Archean terranes, 3.31 ± 0.02 t/m^3 (Griffin et al., 1999b; Poudjom Djomani et al., 2001). The range of SPT mantle densities calculated here for Siberia corresponds to the maximal values of ca. 1.8–3.0% of density deficit with respect to primitive mantle in the Anabar Shield, with a typical value of ca. 0.5–1.5% for most of the Craton interior (Fig. 7d).

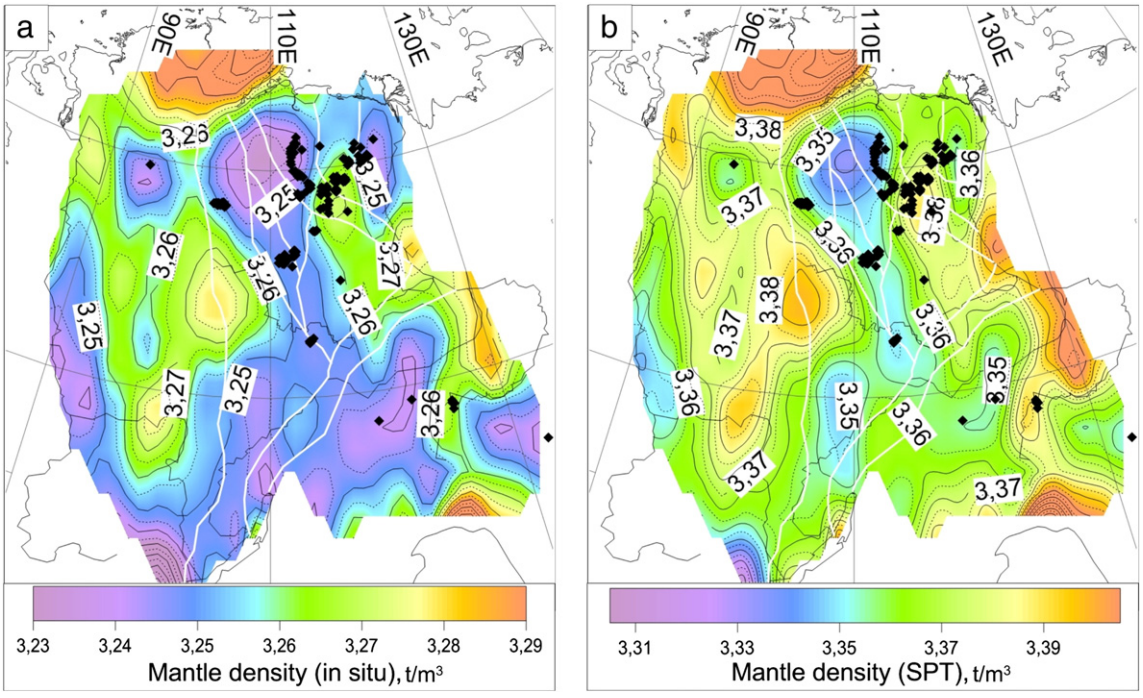

Fig. 5. Modeling results for one-layer Model 1. Average in situ (a) and SPT (b) density structure of the lithospheric mantle (between the Moho and the LAB). White thin lines show the major suture zones of the basement (see Fig. 1a for details). The overall uncertainty in calculated density values is better than 0.02 t/m^3. Symbols — major kimberlite fields.

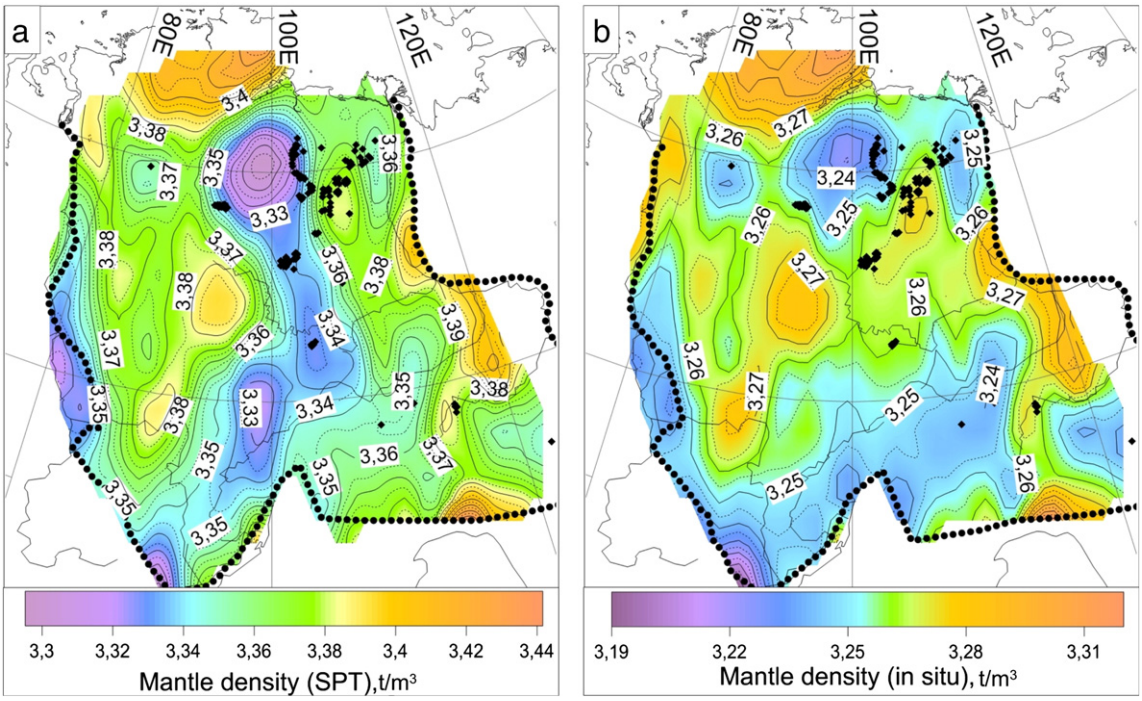

Fig. 6. Modeling results for the upper SCLM layer of Model 2 (see Fig. 4d for explanation). Average in situ (a) and SPT (b) density structure of the lithospheric mantle between the Moho and a 180 km depth. The overall uncertainty of calculated density is better than 0.02 t/m^3. See Fig. S1 for assumed density structure of the bottom SCLM layer (from a 180 km depth down to the LAB). White thin lines show the major suture zones of the basement (see Fig. 1a for details). Dots — major kimberlite clusters. Blue regions in (a) are close to isopycnicity.

A global gravity modeling of SCLM density at SPT conditions indicates that the upper mantle of the Siberian Craton has, on average, density deficit of 1.5–2.3% in case the chemical boundary layer extends down to the base of thermal lithosphere (which corresponds to our Model 1, compare with Fig. 7b) and 1.7–2.4% in case the base of the chemical boundary layer is at a 200 km depth (which is similar to our Model 2, Fig. 7d) (Kaban et al., 2003). Given that the gravity model has a coarser lateral resolution (2° × 2°), is based on a completely different method, and is constrained by a different crustal model (CRUST2.0, Bassin et al., 2000), the two approaches provide extremely similar results for the mantle density structure beneath the Siberian Craton.

4.2. Correlations with tectonics

The density structure of the Siberian lithospheric mantle is well correlated with the tectonic setting. By the amplitude of mantle density anomalies, we recognize three types of cratonic mantle: (i) "pristine" Archean mantle, (ii) cratonic mantle affected by magmatism and sampled by kimberlites, (iii) reworked mantle of rifted parts of the Craton with deep sedimentary basins. We next summarize our results for each of these types, based on the tectonic evolution of the region and the history of rifting and magmatism (Fig. 1b).

4.2.1. "Pristine" Archean mantle

Strongly depleted lithospheric mantle is typical of the shield regions, with a particularly strong density deficit beneath the Anabar Shield (Figs. 5–6), which we attribute to mantle depletion in basaltic components. The removal of basaltic components during mantle melting reduces the mass fraction of Fe, Ca and Al in the residue, while increasing the amount of Mg and thus Mg to Fe ratio. Mineralogically it means that the loss of clinopyroxene and garnet from fertile mantle lherzolite leaves low-density harzburgite, the component minerals of which (olivine and orthopyroxene) are ca. 15% less dense than garnet (Carlson et al., 2005). As a result, density in depleted garnet peridotite is about 2% less than in fertile mantle at the same pressure and temperature conditions.

The maximal values of depletion (density deficit as compared to primitive mantle) at SPT conditions are ca. 2% for Model 1 and 3.2% for the upper layer in Model 2 (Fig. 7b, d). The belt of low dense, depleted lithospheric mantle extends southwards from the Anabar Shield across the central part of the Craton to the Irkutsk Amphitheater (Fig. 2a) north of the Baikal Rift and further to the Biryusa block at the south-western margin of the Craton. Similar low density mantle is typical for the Archean–Proterozoic Angara belt along the western cratonic margin. The two low-dense mantle belts are separated by the Tunguska Basin (a part of the Siberian LIP). The belt of low-dense mantle (density deficit of ca. 2.0–3.2% for Models 1 and 2 beneath the Anabar Shield) corresponds to the region with a very low surface heat flow, and a large amplitude of density anomalies is caused, in part, by a large lithospheric thickness. However, the test model where the lithospheric thickness in the region of low heat flow is set to a constant value of 220 km (Fig. S3a) also indicates low mantle density with a ca. 1.5% density deficit, which is significantly stronger than in the adjacent regions (Fig. S3c).

We thus consider our results as a robust indication that density deficit has the maximum values in the parts of the Siberian Craton that are not sampled by kimberlites (Figs. 5–6). Importantly, for two-layer Model 2, which is supported by petrologic data from cratonic regions worldwide (c.f. Fig. 6.15 in Artemieva, 2011), our calculated values for mantle density deficit for parts of the Craton not sampled by kimberlites are somewhat larger (1.8–3.0%) than those based on petrological data for Archean cratons. Petrologic studies of depleted garnet peridotites report values ranging from 1.4–1.7% (e.g. Pearson et al., 1995; Griffin et al., 1999a) to 2.1–2.2% as compared to primitive mantle (Hawkesworth et al., 1990; Griffin et al., 1998; Poudjom Djomani et al., 2001). The results of earlier geophysical studies (Artemieva, 2003; Kaban et al., 2003) also suggest that the density deficit in the lithospheric mantle may not necessarily correspond to the values expected from petrologic studies of mantle-derived peridotite xenoliths.

Based on buoyancy modeling, which indicates larger density deficit than constrained by xenolith data from Archean cratons, we argue

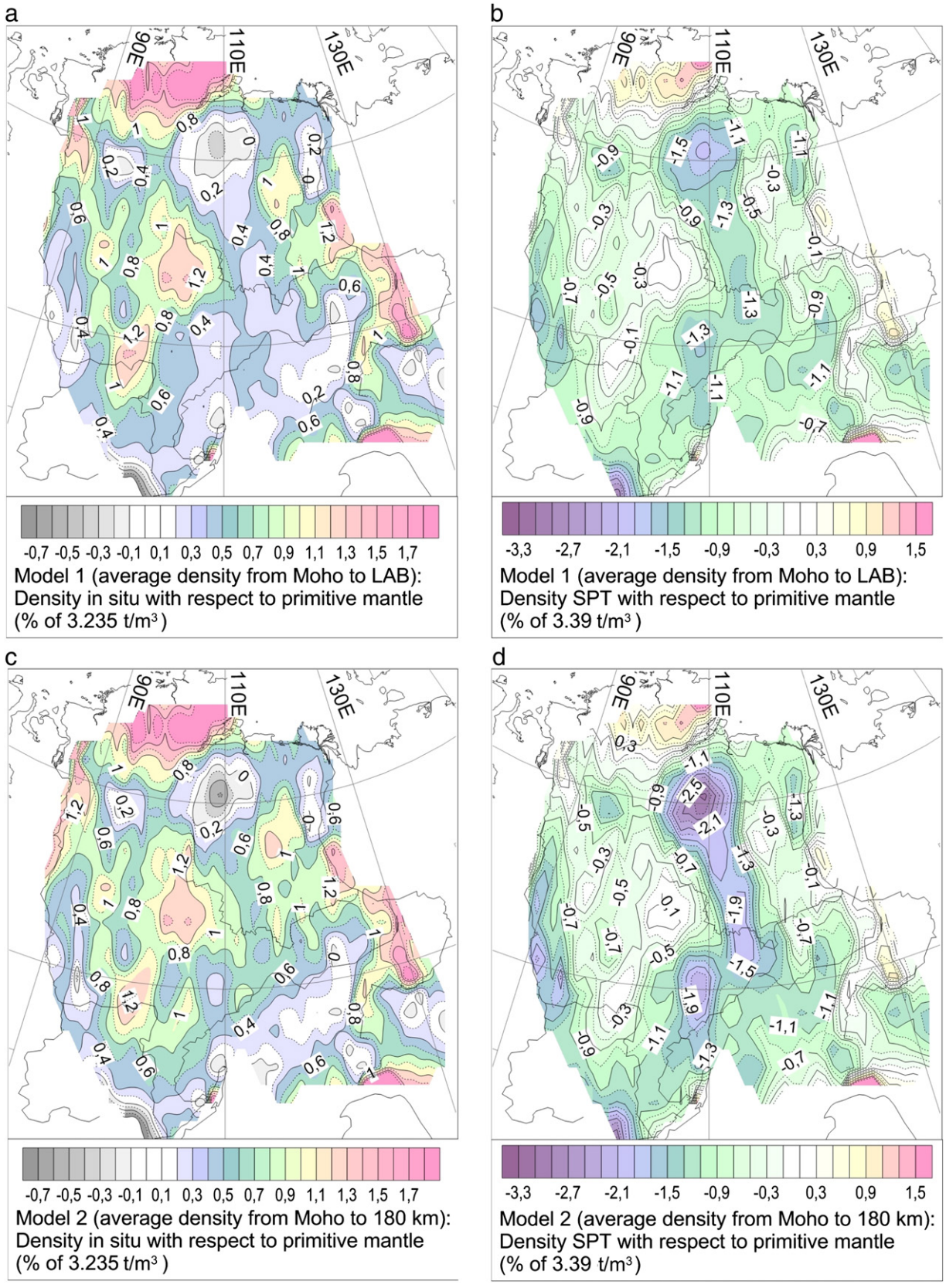

Fig. 7. Mantle density anomalies with respect to primitive mantle. Model 1 (average density from Moho to LAB): (a) In situ average density with respect to primitive mantle (% of 3.24 t/m^3); (b) SPT average density with respect to primitive mantle (% of 3.39 t/m^3). Model 2 (average density from the Moho to 180 km depth): (c) In situ average density with respect to primitive mantle (% of 3.24 t/m^3); (d) SPT average density with respect to primitive mantle (% of 3.39 t/m^3). Regions with near-zero density anomalies at in situ conditions (a, c) are close to isopycnicity. For color figure, please refer to the web version.

that Archean lithospheric mantle sampled by kimberlites has been metasomatically modified and the most depleted cratonic mantle in Siberia is restricted to shield regions with no evidence for earlier magmatism. This observation supports earlier conclusion (Artemieva, 2009, 2011) that xenoliths do not sample most depleted, "pristine" cratonic mantle and thus its composition up to the present remains poorly known.

4.2.2. Cratonic mantle affected by magmatism

Intermediate values of mantle density deficit, 3.34–3.37 t/m^3 at SPT conditions (Model 2) (Fig. 6a), typical of "Proterozoic" SCLM (Griffin et al., 1999a; Poudjom Djomani et al., 2001) are calculated for significant parts of the Craton, in particular for the Proterozoic Akitkan belt, the western part of the Aldan terrane (close to the Vitim Plateau, Fig. 2a), the belt of basement highs along the western margin of the Tunguska Basin, and the Archean–Proterozoic regions sampled by kimberlites.

The largest kimberlite fields (Malo–Botuoba, Daldyn–Alakit) are located in the middle of the relatively low density anomaly (3.34 t/m^3 at SPT, Model 2, which corresponds to ca. 1.5% of density deficit, Fig. 7d), while the kimberlites of the Proterozoic Olenek uplift sample more fertile mantle with average SPT density of 3.37 t/m^3 (ca. 0.6% of density deficit, Models 1 and 2) (Fig. 7b, d). In Model 1, the corresponding density deficit is ca. 0.9% and 0.6% (Fig. 7b).

It is worth noting, that eclogite xenoliths are common for the Siberian kimberlite pipes (Snyder et al., 1997) and thus the presence of high-density material in the Siberian mantle may be expected, at least in regions sampled by kimberlites. Similarly, the Akitkan belt formed by Proterozoic collision of the Archean subcratons may contain entrapped pieces of oceanic lithosphere, and the presence of high-density eclogitic material in its mantle is possible.

The kimberlite fields along the western and eastern margins of the Anabar Shield follow the transition between low- and high-density mantle domains. Unfortunately, studies of mantle xenoliths from the north-central part of the Anabar Shield eastern margin (e.g. the Lower, Middle and Upper Kuonamka kimberlite fields) are not widely discussed in literature and the available results are limited to garnet cumulates. Most garnets are collected from lherzolites at the margin of the field and xenolith P–T arrays indicate a 35–37 mW/m^2 geotherm. The calculated composition of the lithospheric mantle of the Middle Kuonamka field is similar in mean composition to that of the Malo–Botuobiya and Upper Muna fields but the depth of xenolith sampling is limited to 160 km (Griffin et al., 1999b).

Petrological data are, however, available for the kimberlites of the Kharamai field at the south-western edge of the Anabar Shield, where a total of 88 kimberlite pipes and 77 dykes have intruded shortly after the Permo-Triassic eruption of the Siberian Traps (Griffin et al., 2005). The composition of mantle peridotites indicates an increased fertility of the upper part of the SCLM, due to melt-metasomatism, probably associated with the Siberian LIP, which converted harzburgites to lherzolites. Our results indicate that the average SPT density of the SCLM above a 180 km depth (Model 2) is ca. 3.35 t/m^3; however, the exact value can hardly be resolved because the Kharamai field is located at the zone of high gradient in mantle density.

4.2.3. Rifted parts of the Craton

Numerous petrological studies of mantle-derived peridotites from the Siberian Craton and world-wide indicate significant metasomatic enrichment of cratonic mantle during extensional processes. A very fertile mantle with SPT density close to primitive mantle, 3.39 t/m^3, is modeled beneath the parts of the Craton affected by intensive Late Proterozoic–Paleozoic rifting events (Section 2), which led to the formation of deep basins (Figs. 5b, 6b), in particular the Vanavar Basin in the central part of Craton (in the Tunguska Basin) and the Viluy rifted basin at its eastern margin. Similar values of average mantle density are characteristic of the Yenisey–Khatanga trough which marks the northern margin of the Craton.

Importantly, the effect of the Siberian Permo-Triassic event on the mantle density structure is not so prominent (e.g. the inner parts of the Tunguska Basin covered by the traps, Fig. 2b). This suggests that lithospheric mantle beneath the huge cratonic area covered by basaltic lavas has not experienced significant reworking and that the source region of the Siberian LIP event was outside of the Craton. These observations also question the conclusion of Griffin et al. (2005) that melt-metasomatism of cratonic mantle beneath the Kharamai field (the south-western edge of the Anabar Shield) was caused by the eruption of the Siberian Traps.

Based on back-striping analysis of borehole data, two major extensional events (the Cambrian and Devonian) caused subsidence of the Viluy Basin (Polyansky et al., 2013). The next phase (at ca. 250 Ma) of rapid intensive basin subsidence (with a rate of 800–1200 m/My) cannot be explained by rifting, due to the absence of the post-rifting phase of slow subsidence and no indication of temperature increase ca. 90–100 Ma after the main Devonian subsidence (borehole 9, Polyansky et al., 2013). It has long been proposed that phase transitions may have played an important role in the Viluy Basin formation (Artyushkov, 1993). However, until present no geophysical data have supported this hypothesis. Our results, for the first time, document the presence of a high density material (3.39–3.40 t/m^3 at SPT) in the mantle beneath the Viluy Rift (Figs. 5b, 6b), which may be interpreted as evidence for the presence of a partially eclogitized material.

Similarly, the results indicate that several deep basins with the Tunguska Basin and the Yenisey–Khatanga trough are underlain by high density material. Given that calculated densities provide an average over the entire lithospheric column, the presence of even more dense material within a small depth interval cannot be ruled out. Thus our results indicate that intracratonic mantle affected by intensive rifting has been not only metasomatically refertilized, but could have experienced partial or full basalt–eclogite phase transitions at depth interval favorable for this transformation. Following the high density anomalies, one can trace the rifts to the west of the Anabar Shield as well as between the Kureyka and the Tunguska basins.

5. Discussion

5.1. Mantle density at in situ conditions

In situ density of lithospheric mantle is controlled not only by composition but also by temperature (at these depths, the effect of porosity, which is important in shallow crust, is unimportant). Thus in situ density anomalies cannot be directly compared to petrological data, but can be compared to gravity anomalies and seismic velocity structure, assuming that seismic velocities and densities are related (e.g. Ludwig et al., 1970).

The general pattern of in situ (i.e. at ambient P–T conditions within the mantle) density anomalies is similar to the SPT density anomalies, although their amplitude is significantly reduced in regions with cold and thick lithospheric keels. For Model 1, mantle density is in the range from ca. 3.24 t/m^3 to ca. 3.28 t/m^3 (Fig. 5a), whereas for Model 2 density of the upper SCLM layer varies from ca. 3.23 t/m^3 to ca. 3.28 t/m^3 (Fig. 6b), and the maximal difference between Model 1 and the upper layer of Model 2 is less than 0.02 t/m^3 (Fig. S4b). As discussed above, lithospheric temperatures in the interior parts of the Siberian Craton are close to 35–40 mW/m^2 conductive geotherms, which implies average temperature of the SCLM of 800–900 °C. At this mid-lithosphere temperature mantle primitive mantle with a fertile composition would have in situ density of ca. 3.283–3.295 t/m^3.

Given a very small range of in situ density variations within the Craton interior and a significant scatter in velocity–density relationship (Barton, 1986), one cannot predict seismic velocity anomalies from density anomalies. A direct comparison of free-board modeling results with seismic velocity models is further hampered by the fact that density anomalies are depth-integrated and refer to the entire lithospheric

column, rather than to any particular depth in the mantle. As a rough comparison between density and seismic velocities, we note that 3.24–3.28 t/m^3 calculated from buoyancy (Model 1) or gravity corresponds to P-wave velocity of ca. 7.9–8.1 km/s (or 7.1–8.9 km/s including outliers in the velocity–density relationship) (Lowrie, 2007). The predicted values for Vp velocities are somewhat smaller than in interpretations of seismic long-range Soviet PNE profiles across the Siberian Craton, which at a 50–180 km depth indicate Vp velocities in the range 8.1–8.4 km/s beneath the Tunguska and Viluy basins, profile Craton (Egorkin et al., 1987) and in the range 8.1–8.55 km/s beneath the Anabar Shield, profile Horizont (Burmakov et al., 1987). Along these profiles, low Vp velocities (8.1–8.2 km/s), comparable to predictions based on average SCLM density, are usually restricted to the depth range of ca. 90–140 km. Recently, an attempt has been made to interpret Vp-velocities along the long-range seismic profiles Kimberlite and Meteorite in terms of thermal and density structure of the mantle beneath the Siberian Craton, with account for petrological data on depleted garnet peridotite xenoliths and primitive mantle composition (Kuskov et al., 2014). Those authors conclude that compositionally distinct mantle layers cannot be recognized by seismic methods.

The number of gravity studies of mantle heterogeneity beneath Siberia is limited (e.g. Romanyuk, 1995; Yegorova and Pavlenkova, 2014), and they are often constrained by the PNE seismic profiles. Seismic P-wave velocity structure along the PNE profiles Quartz, Craton and Kimberlite has been recently used to perform a 2D gravity modeling for the Siberian Craton (Yegorova and Pavlenkova, 2014). Our results challenge the conclusions of this gravity modeling which, based on low Vp beneath the Viluy Basin (with the lowest Vp in the lithosphere of the entire Siberian Craton), were interpreted as the most depleted cratonic mantle in Siberia (Yegorova and Pavlenkova, 2014). However, temperature- and compositional effects on seismic velocities and density are significantly different (Artemieva, 2009). In particular, low seismic velocities can be caused by a large number of factors other than compositional heterogeneity (anisotropy, fluids, melts, etc.) which may not necessarily require low mantle density (c.f. Artemieva, 2011).

5.2. Mantle in situ density and isopycnicity

In situ mantle density is directly related to isopycnicity. According to the isopycnic (equal-density) hypothesis (Jordan, 1975), a density increase in cratonic upper mantle caused by low temperatures is closely compensated by a density decrease caused by compositional differences. The presence of compositionally distinct chemical boundary layer (CBL) in the subcontinental lithospheric mantle (SCLM) provides its buoyancy and preservation of thick lithospheric roots over long geological times (Jordan, 1988; Lee, 2006).

Whether or not the isopycnic condition is satisfied in the cratonic lithosphere in general (Kaban et al., 2003), or at any depth (Kelly et al., 2003), or over all tectonic history of the cratons (Eaton and Perry, 2013) is a subject of debate. For example, a global gravity modeling suggests that density variations due to temperatures are ca. 40% larger than the variations due to compositional differences (Kaban et al., 2003), in contrast to the classical isopycnic theory which predicts a complete depletion-temperature balance in the cratonic lithosphere at any depth. Numerical modeling of stability, density, temperature and viscosity of the cratonic root beneath the Kaapvaal Craton provides another argument against the isopycnic hypothesis (Eaton and Perry, 2013).

Studies of the mantle xenoliths from kimberlite pipes of the Kaapvaal Craton show that the distribution of density in the mantle deviates from the ideal isopycnic correlation of mantle temperature and density (Kelly et al., 2003). These authors calculated mantle density from whole rock composition using the relationship between whole rock Mg# and normative density (Jordan, 1988). They found that mantle xenoliths derived from above a 200 km depth are positively buoyant, while xenoliths from the deeper mantle are negatively buoyant, making the whole cratonic lithospheric mantle neutrally buoyant. Similar observations were reported for peridotites from the Tanzanian Craton (Lee and Rudnick, 1999).

Importantly, a very high density mantle material (e.g. dunites) is present in mantle xenoliths only in very small quantities and its true amount in the mantle is unknown. This makes a bias in comparing the SCLM density calculated from geophysical and petrological data. Analysis of garnet in mantle peridotites from Kaapvaal shows the presence of a very depleted (with SPT density as low as 3.1 t/m^3) mantle at a depth range 120–160 km and a very dense root with density reaching 3.4–3.44 t/m^3 at ca. 180 km depth (Griffin et al., 2003; James et al., 2004). Similar results (with density of 3.42 t/m^3 at 200 km depth) are constrained by limited data on high-T garnet peridotites from the deepest part of the Kaapvaal lithospheric mantle (James et al., 2004). The average Mg# of deformed Siberian peridotites (the Udachnaya kimberlite pipe of the Daldyn terrane) from a depth of 200–220 km ranges from ca. 87 to 91 (Agashev et al., 2013) which implies average SPT density of 3.37–3.45 t/m^3, i.e. similar to or denser than the asthenospheric mantle. These results indicate that mantle density constrained by mantle xenoliths from kimberlite pipes deviates from the isopycnic conditions (Lee and Rudnick, 1999; Kelly et al., 2003).

Besides vertical stratification of the lithospheric mantle and deviations of the vertical density profile from isopycnicity, lateral density heterogeneity associated with the age of the SCLM (Griffin et al., 1999b; Poudjom Djomani et al., 2001) and its tectonic evolution (Section 4) contributes to the complexity of cratonic isopycnicity. Given that our results provide density values integrated over the lithosphere depth, we cannot test if the isopycnic condition is fulfilled over the vertical structure of the SCLM. However, we can examine if "bulk" isopycnicity is fulfilled for the Siberian mantle.

As discussed in Section 3, in situ density of primitive mantle at sublithospheric temperatures (1300 °C) is assumed to be 3.235 t/m^3. However, average in situ density values calculated for the Siberian mantle are significantly higher, within the range of ca. 3.24–3.28 t/m^3 for Models 1 and 2. Note that the total range of possible in situ density variations (0.04 t/m^3) is larger than the overall uncertainty of the density model (better than 0.02 t/m^3), and thus the anomalies in the mantle density structure are well resolved. The range of in situ density variations (0.04 t/m^3 or 1.2% with respect to primitive mantle) is 2–3 times less than at SPT conditions (2.3% for Model 1 to 3.2% for Model 2), due to temperature compensation of compositional density anomalies (Fig. 7). However, even at in situ temperatures the compensation is incomplete, the isopycnic condition is not fully satisfied for significant parts of the Siberian Craton, and there are significant lateral variations in the extent to which isopycnicity is achieved (Fig. 7a, c).

For example, the region of the Anabar Shield and the southern parts of the Craton have in situ average density close to in situ asthenospheric (ca. 3.235 t/m^3), suggesting isopycnic condition is nearly satisfied there. These regions also have a near-zero density anomaly as compared to primitive mantle at in situ conditions (Fig. 7a, c). At the same time, most of the Craton has positive relative density anomalies at in situ conditions, both for Model 1 and 2, providing a clear evidence that, integrated over the entire lithospheric column, the Siberian mantle does not comply with the isopycnic condition. Regions sampled by kimberlites have moderate deviations from "bulk" isopycnicity, while significant deviations are expected for the cratonic regions that have experienced intensive rifting (the Viluy Rift) and basin subsidence (the Vanavar and the Kansk–Taseev basins). We thus conclude, based on the results for the Siberian Craton, that the extent to which the isopycnic condition is satisfied depends on the degree of lithosphere reworking: while a close balance between thermal and compositional density deviations may be expected for depleted or weakly refertilized cratonic mantle, apparently it cannot be expected for significantly reworked, nearly fertile cratonic lithosphere typical of deep intracratonic basins.

5.3. Mantle density and lateral Mg# variations

Assuming that mantle density variations are caused by mantle depletion (refertilization) and are directly controlled by the amount of iron in the mantle, we next convert SPT density anomalies to Mg# number, assuming the isopycnic density–Mg# correlation (Jordan, 1988). This correlation is constrained by density values calculated from whole rock oxide composition for 78 samples of (both low-T and high-T) garnet lherzolites from Kaapvaal (Jordan, 1979) and ignores variations in alumina content. Note that since the isopycnic condition is not fully satisfied for much of the Craton (Section 5.2), this conversion of mantle density to Mg# is, strictly speaking, inaccurate. Given that mantle density is the integral value for the entire lithospheric column, the calculated mantle Mg# also provides the average value for the entire lithospheric mantle down to the LAB (Model 1) (Fig. 8a) and for the upper layer down to 180 km depth (Model 2) (Fig. 8b), and thus its comparison with petrological data is limited.

A comparison of "synthetic" and petrologic Mg-numbers leads to several major conclusions. The calculated values of Mg# for average bulk lithospheric mantle are in the range typically calculated from petrological studies of mantle-derived peridotite xenoliths, but parts of the Craton with the largest "synthetic" Mg# (ca. 92–93) are not sampled by mantle xenoliths and cannot be compared to petrologic data. The part of the Craton unaffected by any large magmatic events and melt-metasomatism, has the highest values of bulk mantle depletion (e.g. ca. 92.5 in the mantle beneath the Anabar Shield for Model 1 and 93.5 for Model 2), which implies a high concentration of depleted harzburgites.

In contrast, the deep intracratonic basins (e.g. Vanavar and Viluy) have mantle with bulk Mg# of ca. 89.5. These values indicate fertile composition of the mantle, which may be produced by a large scale metasomatic modification of the entire cratonic lithosphere during large-scale rifting processes (recall that our "synthetic" Mg# are averaged for the entire lithospheric column).

Similar to the pattern of density anomalies, the SCLM beneath the Siberian kimberlite fields has intermediate values of Mg#, ca. 91. A comparison with the average mantle Mg# (from the Moho down to petrological LAB) calculated from garnet concentrates (Griffin et al., 1999a, b, 2005) shows a good agreement for the Malo–Botuoba kimberlite field and the north-eastern end of the Olenek trend. Similarly, garnet peridotites from the Kharamai kimberlite field at the south-western margin of the Anabar Shield provide 92 for Fo in olivine at depths of 90–180 km with a sharp decrease to 90 at ca. 190 km depth (Griffin et al., 2005), while our calculation indicates "bulk" Mg# of ca. 91–92.

Two-layer Model 2 has a better agreement with the petrological Mg# for the Daldyn–Alakit field. This observation supports the thermal model (Artemieva, 2006) which indicates that this region has a ca. 350 km thick lithosphere (TBL), while the CBL base is reached already at a 150–180 km depth (Artemieva, 2009), in agreement with petrological data which indicates the start of metasomatic enrichment at a 160–180 km depth (the deepest xenoliths are from a 250 km depth, Griffin et al., 1999b).

Petrologic data indicate a strong short-wavelength (<100 km) lateral heterogeneity of the Siberian SCLM, while "synthetic" Mg-numbers (although calculated on a 1° × 1° grid) show a smooth pattern with a typical wavelength of compositional anomalies of ca. 300–500 km. In particular, xenoliths from the Olenek province indicate highly heterogeneous Mg#, with very depleted values in its central part. "Synthetic" Mg# values constrained by mantle density provide a smeared picture, but indicate the presence of enriched mantle material, in agreement with petrologic data from two Mesozoic kimberlite fields in the same region (Fig. 8). Note that region with the strongest heterogeneity in petrologic Mg# (the Proterozoic Hapchan and Birekte terranes) has increased mantle density (Figs. 5, 6), interpreted as caused by melt-metasomatism. This process may produce a spatially heterogeneous pattern with small bodies of highly metasomatized material embedded into otherwise still depleted cratonic mantle.

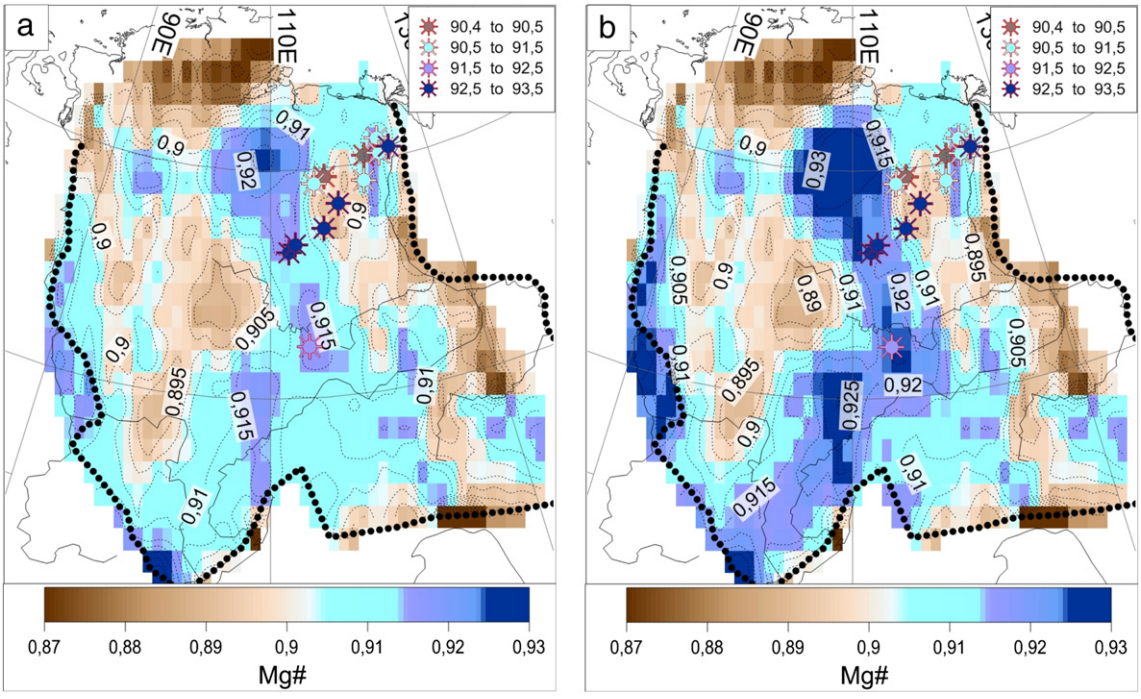

Fig. 8. Mg# number of the lithospheric mantle calculated on a 1° × 1° grid from mantle densities (using the isopycnic relation between density and Mg#, Jordan, 1988): (a) for one-layer Model 1 where Mg# is average for the entire lithospheric column and (b) for the upper layer of Model 2 where Mg# is average for the top SCLM layer (between the Moho and a 180 km depth). Colored symbols — Mg# based on petrologic data for the Siberian lithospheric mantle (Griffin et al., 1999b). For consistency of comparison, colors indicate the value of petrologic Mg# averaged over the SCLM depth. Note that while Mg# calculated from density refers to the bulk mantle composition, petrologic Mg# are calculated from garnets in mantle-derived peridotite xenoliths, and thus represent only a part (most likely 70–80%) of the SCLM composition.

6. Conclusions

The nearly isostatic balance of the Siberian Craton allow us to apply the free-board modeling to calculate the density structure of the lithospheric mantle beneath the Craton. Availability of the reliable regional crustal model and the thermal model of the lithospheric mantle secures high reliability of free-board modeling, with the overall uncertainty of mantle density better than 0.02 t/m^3 or better than ca. 0.6% with respect to primitive mantle. Mantle density is calculated for two models of the chemical boundary layer: (i) between the Moho and the base of thermal lithosphere, LAB (Model 1) and (ii) between the Moho and a 180 km depth (Model 2) with fixed, nearly fertile, density value in the layer below 180 km depth down to the LAB. The results, calculated at in situ and at room temperature (SPT) conditions, show the following.

1) Density structure of the Siberian lithospheric mantle is heterogeneous and, in agreement with petrologic data, is in the range from ca. 3.23–3.24 t/m^3 to ca. 3.28 t/m^3 (in situ) for both models.
2) We observe a strong correlation between the density structure and the tectonic setting and, by density values, distinguish three types of cratonic lithospheric mantle: "pristine" Archean mantle, metasomatized cratonic mantle affected by magmatism and sampled by kimberlites, reworked mantle of intracratonic rifts and deep sedimentary basins.
   The maximum values of mantle density deficit (1.8–3.0% as compared to primitive mantle) are observed for parts of the Craton that are not sampled by kimberlites (tectonically most preserved cratonic lithosphere of the Anabar and Aldan Shields). Mantle depletion calculated for these shield regions is larger than based on petrological studies of mantle-derived peridotites (Pearson et al., 1995; Griffin et al., 1998; Djomani et al., 2001).
   Most of the cratonic mantle has a typical density deficit of ca. 1.0–1.5% with respect to primitive mantle. Mantle density beneath the kimberlite fields is more dense (more fertile) than "pristine" mantle of the Anabar Shield, in agreement with earlier conclusions that composition of "pristine" cratonic mantle up to date remains poorly known (Artemieva, 2009, 2011).
   The deepest intracratonic sedimentary basins (the Varnavar and the Viluy Basins) are underlined by a high-density mantle (3.38–3.4 t/m^3), which may be indicative not only of the metasomatic melt-enrichment but also of the presence of eclogitic material in the lithospheric mantle of these rifts.
   The inner parts of the Tunguska Basin covered by a thick sequence of the Siberian traps have intermediate values of mantle density. This suggests that the effect of the Siberian Permo-Triassic event on the mantle density structure is modest and that the source region of the Siberian LIP event lies outside of the Craton interior.
3) Our results indicate that isopycnic condition is not entirely satisfied for significant parts of the Siberian mantle. Significant lateral variations in the degree to which isopycnicity is satisfied are correlated with mantle depletion/refertilization. The best agreement with the isopycnic condition is observed for the Anabar Shield region and some other depleted or weakly refertilized cratonic keels. However, a close balance between thermal and compositional density deviations may not be expected for nearly fertile cratonic lithosphere typical of deep rifted basins.
4) Cratonic regions with a strong short-wavelength heterogeneity in petrological Mg# have intermediate values of mantle density anomalies. We speculate that local infiltration of fluids and melts into the cratonic mantle could produce small-scale patches of highly metasomatized material within an overall depleted cratonic mantle, averaged to intermediate values in geophysical models. Xenoliths from such a region may provide incomplete picture on mantle composition strongly biased by kimberlite sampling.

Acknowledgments

Funding of YC through the grants FNU-10-083081, DFF-1323-00053 (Denmark) and the Faculty of Science, University of Copenhagen to IMA is gratefully acknowledged. Editorial suggestions from R. Keller and anonymous reviewer are acknowledged.

Appendix A. Free-board method

Surface topography (*Ho*) results from the crustal and lithospheric buoyancies and dynamic topography caused by mantle flow. Since the study region is close to isostatic equilibrium (Fig. 2b), the effect of dynamic topography is neglected, so that $Ho = Bc + Bm - D$, where *Bc* and *Bm* are crustal and lithospheric buoyancies, respectively, and D is a free parameter which is the isostatic height of sea level above the asthenosphere. In the present study we adopt the value of D = 4.25 km and justify its choice in Section 3.2. The details of model assumptions and parameterization are presented in Section 3. Fig. A1 illustrates the modeling approach, which follows Lachenbruch and Morgan (1990).

Crustal and lithospheric mantle contributions to topography are caused by variations in thickness (*Hc* and *Hm*) and in situ density (ρ_c and ρ_m) of the crust and the lithospheric mantle, respectively: $Bc = Hc\,(\rho_a - \rho_c)\,/\,\rho_a$, and $Bm = Hm\,(\rho_a - \rho_m)\,/\,\rho_a$, where ρ_a is density of asthenosphere (the sublithospheric mantle) assumed to be constant. The SPT (at room P–T conditions) density can be calculated from in situ density by introducing correction for thermal expansion, which for the lithospheric mantle is: $\rho_m = \rho_{mo}\,[1 - \alpha\,(T_M + T_{LAB})\,/\,2]$, where ρ_{mo} is SPT density of the lithospheric mantle, T_M and T_{LAB} are temperatures at the base of the crust (laterally variable) and the base of the lithosphere (assumed to be constant), and $\alpha = 3.5 \times 10^{-5}$ 1 / K is the thermal expansion coefficient of mantle peridotite.

Appendix B. Supplementary data

Supplementary data to this article can be found online at http://dx.doi.org/10.1016/j.gr.2014.10.002.

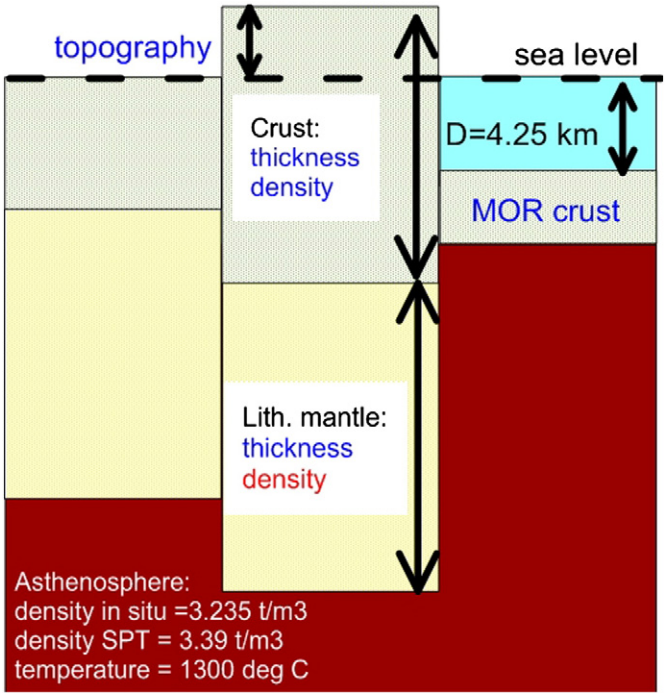

Fig. A1. Sketch illustrating model specification for density calculations. Text in blue refers to known parameters, in red — to unknown. Density and temperature of the asthenosphere are assumed and fixed. D — fixed model parameter which is the isostatic height of sea level above the asthenosphere (see Fig. S2 for details).

References

Agashev, A.M., Ionov, D.A., Pokhilenko, N.P., Golovin, A.V., Cherepanova, Yu., Sharygin, I.S., 2013. Metasomatism in lithospheric mantle roots: constraints from whole-rock and mineral chemical composition of deformed peridotite xenoliths from kimberlite pipe Udachnaya. Lithos 160–161, 201–215.

Amante, C., Eakins, B.W., 2009. ETOPO1 1 arc-minute Global Relief Model: Procedures, Data Sources and Analysis. NOAA Technical Memorandum NESDIS NGDC-24. National Geophysical Data Center, NOAA http://dx.doi.org/10.7289/V5C8276M, ([access date]).

Anderson, D.L., 1987. Thermally induced phase changes, lateral heterogeneity of the mantle, continental roots, and deep slab anomalies. Journal of Geophysical Research 92, 13968–13980.

Artemieva, I.M., 2003. Lithospheric structure, composition, and thermal regime of the East European Craton: implications for the subsidence of the Russian Platform. Earth and Planetary Science Letters 213, 429–444.

Artemieva, I.M., 2006. Global 1° × 1° thermal model TC1 for the continental lithosphere: implications for lithosphere secular evolution. Tectonophysics 416, 245–277.

Artemieva, I.M., 2007. Dynamic topography of the East European Craton: shedding light upon lithospheric structure, composition and mantle dynamics. Global and Planetary Change 58 (2007), 411–434.

Artemieva, I.M., 2009. The continental lithosphere: reconciling thermal, seismic, and petrologic data. Lithos 109, 23–46. http://dx.doi.org/10.1016/j. lithos. 2008.09.015.

Artemieva, I.M., 2011. The Lithosphere: An Interdisciplinary Approach. Monograph. Cambridge University Press 9780521843966, (794 pp.).

Artemieva, I.M., Mooney, W.D., 2001. Thermal structure and evolution of Precambrian lithosphere: a global study. Journal of Geophysical Research 106, 16387–16414.

Artemjev, M.E., Kaban, M.K., Kucherinenko, V.A., Demyanov, G.V., Taranov, V.A., 1994. Subcrustal density inhomogeneities of Northern Eurasia as derived from the gravity data and isostatic models of the lithosphere. Tectonophysics 240, 249–280.

Artyushkov, E.V., 1993. Physical Tectonics. Russian Academy of science, NAUKA, Moscow (456 pp.).

Ashchepkov, I.V., Pokhilenko, N.P., Vladykin, N.V., et al., 2010. Structure and evolution of the lithospheric mantle beneath Siberian Craton, thermobarometric study. Tectonophysics 485, 17–41.

Ashchepkov, I.V., Nigmatulina, E.N., Khmelnikova, O.S., et al., 2013. Regularities and mechanism of formation of the mantle lithosphere structure beneath the Siberian Craton in comparison with other cratons. Gondwana Research 23 (1), 4–24. http://dx.doi.org/10.1016/j.gr.2012.03.009.

Barton, P.J., 1986. The relationship between seismic velocity and density in the continental crust — a useful constraint? Geophysical Journal of the Royal Astronomical Society 87, 195–208.

Bassin, C., Laske, G., Masters, G., 2000. The current limits of resolution for surface wave tomography in North America. Eos, Transactions of the American Geophysical Union 81, F897.

Beard, B.L., Fraracci, K.N., Taylor, L.A., Snyder, G.A., Clayton, R.N., Mayeda, T.K., Sobolev, N.V., 1996. Petrography and geochemistry of eclogites from the Mir kimberlite, Yakutia, Russia. Contributions to Mineralogy and Petrology 125, 293–310.

Boyd, F.R., 1989. Compositional distinction between oceanic and cratonic lithosphere. Earth and Planetary Science Letters 96, 15–26.

Boyd, F.R., 1997. Origin of peridotite xenoliths: major element considerations. In: Ranalli, G., et al. (Eds.), High Pressure and High Temperature Research on Lithosphere and Mantle Materials. University of Siena.

Boyd, F.R., McCallister, R.H., 1976. Densities of fertile and sterile garnet peridotites. Geophysical Research Letters 3, 509–512.

Boyd, F.R., Pokhilenko, N.P., Pearson, D.G., Mertzman, S.A., Sobolev, N.V., Finger, L.W., 1997. Composition of the Siberian cratonic mantle: evidence from Udachnaya peridotite xenoliths. Contributions to Mineralogy and Petrology 128, 228–246.

Burmakov, Y.A., Chernyshev, N.M., Vinnik, L.P., Egorkin, A.V., 1987. Comparative characteristics of the lithosphere of the Russian Platform, the West Siberian Platform and the Siberian Platform from seismic observations on long-range profiles. In: Kroner, A. (Ed.), Proterozoic Lithospheric Evolution. AGU, Geodynam. Ser. v. 17, pp. 175–189.

Carlson, R.W., Pearson, G., James, D.E., 2005. Physical, chemical, and chronological characteristics of continental mantle. Reviews of Geophysics 43, RG1001. http://dx.doi.org/10.1029/2004RG000156.

Cherepanova, Y., Artemieva, I., Thybo, H., Chemia, Z., 2013. Crustal structure of the Siberian Craton and the West Siberian basin: an appraisal of existing seismic data. Tectonophysics 609, 154–183.

Christensen, N.I., Mooney, W.D., 1995. Seismic velocity structure and composition of the continental crust: a global view. Journal of Geophysical Research 100, 9761–9788.

Condie, K.C., Rosen, O.M., 1994. Laurentia–Siberia connection revisited. Geology 22, 168–170.

Courtillot, V., Kravchinsky, V.A., Quidelleur, X., Renne, P.R., Gladkochub, D.P., 2010. Preliminary dating of the Viluy traps (Eastern Siberia): eruption at the time of Late Devonian extinction events? Earth and Planetary Science Letters 300, 239–245.

Davis, G.L., Sobalev, N.V., Kharkiv, A.D., 1980. New data on the age of Yakutian kimberlites obtained by the uranium–lead method on zircon. Doklady Akademii Nauk SSSR 254, 53–57.

Djomani, Y.H.P., et al., 2001. The density structure of subcontinental lithosphere through time. EPSL 184, 605–621.

Eaton, D.W., Perry, H.K.C., 2013. Ephemerical isopycnicity of cratonic mantle keels. Nature Geoscience 6 (11), 967–970.

Egorkin, A.V., Zuganov, S.K., Pavlenkova, N.A., Chernyshev, N.M., 1987. Results of lithospheric studies from long-range profiles in Siberia. Tectonophysics 140, 29–47.

Fedorenko, V.A., Lightfoot, P.C., Naldrett, A.J., Czamanske, G.K., Hawkesworth, C.J., Wooden, J.L., Ebel, D.S., 1996. Petrogenesis of the flood basalt sequence at Noril'sk, North Central Siberia. International Geology Review 38, 99–135.

Foulger, G.R., Panza, G.F., Artremieva, I.M., Bastow, I.D., Cammarano, F., Evans, J.R., Hamilton, W.B., Julian, B.R., Lustrino, M., Thybo, H., Yanovskaya, T.B., 2013. Caveats on tomographic images. Terra Nova 25 (4), 259–281.

Fuchs, K., Wenzel, F., 1997. Conservation of lithospheric DSS data. In: Fuchs, K. (Ed.), Upper Mantle Heterogeneities from Active and Passive Seismology. Kluwer Academic Publishers, pp. 11–31.

Gaul, O.F., Griffin, W.L., O'Reilly, S.Y., Pearson, N.J., 2000. Mapping olivine composition in the lithospheric mantle. Earth and Planetary Science Letters 182, 223–235.

Gladkochub, D., Pisarevsky, S.A., Donskaya, T., Natapov, L.M., Mazukabzov, A., Stanevich, A., Slkyarov, E., 2006. Siberian Craton and its evolution in terms of Rodinia hypothesis. Episodes 29 (3), 169–174.

Gladkochub, D.P., Donskaya, T.V., Mazukabzov, A.M., Stanevich, A.M., Sklyarov, E.V., Ponomarchuk, V.A., 2007. Signature of Precambrian extension events in the southern Siberian Craton. Russian Geology and Geophysics 48, 17–31.

Griffin, W.L., O'Reilly, S.Y., Ryan, C.G., Gaul, O., Ionov, D., 1998. Secular variation in the composition of subcontinental lithospheric mantle. In: Braun, J., et al. (Eds.), Structure and Evolution of the Australian Continent. Geodynamics Series, Am. Geophys. Union 26, pp. 1–25.

Griffin, W.L., O'Reilly, S.Y., Ryan, C.G., 1999a. The composition and origin of subcontinental lithospheric mantle. In: Fei, Y., Bertka, C.M., Mysen, B.O. (Eds.), Mantle Petrology: Field Observations and High-pressure Experimentation: A Tribute to Francis R. (Joe) BoydGeochemical Society Special Publication #6. The Geochemical Society, Houston, TX, pp. 13–45.

Griffin, W.L., Ryan, C.G., Kaminsky, F.V., et al., 1999b. The Siberian lithosphere traverse: mantle terranes and the assembly of the Siberian Craton. Tectonophysics 310, 1–35.

Griffin, W.L., O'Reilly, S.Y., Abe, N., et al., 2003. The origin and evolution of Archean lithospheric mantle. Precambrian Research 127, 19–41.

Griffin, W.L., Natapov, L.M., O'Reilly, S.Y., et al., 2005. The Kharamai kimberlite field, Siberia: modification of the lithospheric mantle by the Siberian Trap event. Lithos 81, 167–187.

Hawkesworth, C.J., Kempton, P.D., Rogers, N.W., Ellam, R.M., van Calsteren, P.W., 1990. Continental mantle lithosphere, and shallow level enrichment process in the Earths mantle. Earth and Planetary Science Letters 96, 256–268.

Henkel, H., 1994. Standard diagrams of magnetic properties and density: a tool for understanding magnetic petrology. Journal of Applied Geophysics 32, 43–53.

Herceg, M., Artemieva, I.M., Thybo, H., Cherepanova, Yu., 2014. Density heterogeneity of the lithospheric mantle in the Siberian Craton from satellite gravity and a new regional crustal model. JGR (submitted for publication).

Ilupin, I.P., Vaganov, V.I., Prokpuck, B.I., 1990. Kimberlites. Nedra Publishing House, Moscow (248 pp. (in Russian)).

Ionov, D.A., Doucet, L.S., Ashchepkov, I.V., 2010. Composition of the lithospheric mantle in the Siberian Craton: new constraints from fresh peridotites in the Udachnaya-East Kimberlite. Journal of Petrology 51 (11), 2177–2210.

Irifune, T., 1987. An experimental investigation of the pyroxene–garnet transformation in a pyrolite composition and its bearing on the composition of the mantle. Physics of the Earth and Planetary Interiors 45, 324–336.

James, D., Boyd, F., Schutt, D., Bell, D., Carlson, R., 2004. Xenolith constraints in seismic velocities in the upper mantle beneath southern Africa. Geochemistry, Geophysics, Geosystems 5. http://dx.doi.org/10.1029/2003GC000551.

Jordan, T.H., 1975. The continental tectosphere. Reviews of Geophysics and Space Physics 13, 1–12.

Jordan, T.H., 1979. Mineralogies, densities and seismic velocities of garnet lherzolites and their geophysical implications. In: Boyd, F.R., Meyer, H.O.A. (Eds.), The Mantle Sample: Inclusions in Kimberlites and other Volcanics. Am. Geophys. Union, Washington, DC, pp. 1–14.

Jordan, T.H., 1988. Structure and formation of the continental tectosphere. Journal of Petrology 11–37 (Special lithosphere issue).

Kaban, M.K., Schwintzer, P., Artemieva, I.M., Mooney, W.D., 2003. Density of the continental roots: compositional and thermal effects. Earth and Planetary Science Letters 209, 53–69.

Kelly, R.K., Kelemen, P.B., Jull, M., 2003. Buoyancy of the continental upper mantle. Geochemistry, Geophysics, Geosystems (ISSN: 1525-2027) 4 (2), 1017. http://dx.doi.org/10.1029/2002GC000399.

Kopylova, M.G., McCammon, C., 2003. Composition and the Redox State of the Slave Peridotitic Mantle. Proc. 8th Intern. Kimberlite Conf., Victoria, BC, Canada, June 2003: FLA-0195.

Kuskov, O.L., Kronrod, V.A., Prokof'ev, A.A., Pavlenkova, N.I., 2014. Petrological–geophysical models of the internal structure of the lithospheric mantle of the Siberian Craton. Petrology 22 (1), 17–44.

Kustowski, B., Ekstrom, G., Dziewonski, A.M., 2008. The shear-wave velocity structure in the upper mantle beneath Eurasia. Geophysical Journal International 174, 978–992.

Kuznetsov, V.G., 1997. Riphean hydrocarbon reservoirs of the Yurubchen–Tokhom zone, Lena–Tunguska province, NE Russia. Journal of Petroleum Geology 20 (4), 459–474.

Lachenbruch, A.H., Morgan, P., 1990. Continental extension, magmatism and elevation; formal relations and rules of thumb. Tectonophysics 174, 39–62.

Laske, G., Masters, G., Ma, Z., Pasyanos, M., 2013. Update on CRUST1.0 — a 1-degree global model of Earth's crust. Geophysical Research Abstracts 15 (Abstract EGU2013-2658).

Lee, C.-T.A., 2006. Geochemical/petrologic constraints on the origin of cratonic mantle. In: Benn, K., Mareschal, J.-C., Condie, K.C. (Eds.), Archean Geodynamics and Environments. American Geophysical Union, Geophysical Monograph Series 164.

Lee, C.-T., Rudnick, R.L., 1999. Compositionally stratified cratonic lithosphere: petrology and geochemistry of peridotite xenoliths from the Labait tuff cone, Tanzania. In:

Gurney, J.J., Richardson, S.R. (Eds.), Proc. 7th Int. Kimberlite Conference. Red Roof Designs, Cape Town, pp. 503–521.
Legendre, C.P., Meier, T., Lebedev, S., Friederich, W., Viereck-Götte, L., 2012. A shear wave velocity model of the European upper mantle from automated inversion of seismic shear and surface waveforms. Geophysical Journal International 191, 282–304.
Levshin, A.L., Ritzwoller, M.H., Barmin, M.P., Villasenor, A., Padgett, C.A., 2001. New constraints on the arctic crust and uppermost mantle: surface wave group velocities, Pn, and Sn. Physics of the Earth and Planetary Interiors 123, 185–204.
Lowrie, W., 2007. Fundamentals of Geophysics. Cambridge University Press, p. 390.
Ludwig, W.F., Nafe, J.E., Drake, C.L., 1970. Seismic refraction. In: Maxwell, A.E. (Ed.), The Sealdeas and Observations on Progress in the Study of the Seas v. 4. Wiley-Interscience, New York, pp. 53–84.
Meert, J.G., 2002. Paleomagnetic evidence for a Paleo-Mesoproterozoic supercontinent, Columbia. Gondwana Research 5, 207–215.
Milanovsky, E.E., 1996. Geology of Russia and Adjacent Areas (Northern Eurasia). Moscow University Press, Moscow (in Russian).
O'Brien, H., Lehtonen, M., Spencer, R., Birnie, A., 2003. Lithospheric mantle in eastern Finland: a 250 km 3D transect. Proc. 8th Int. Kimberlite Conf., Victoria, BC, Canada, June 2003: FLA–0261.
Pail, R., Bruinsma, S., Migliaccio, F., Foerste, C., Goiginger, H., Schuh, W.-D., Höck, E., Reguzzoni, M., Brockmann, J.M., Abrikosov, O., Vicherts, M., Fecher, T., Mayrhofer, R., Krasbutter, I., Sanso, F., Tscherning, C.C., 2011. First GOCE gravity field models derived by three different approaches. Journal of Geodesy 85, 819–843.
Parfenov, L.M., Kuz'min, M.I., 2001. Tectonics, Geodynamics, and Metallogeny of the Sakha (Yakutia) Republic. MAIK Nauka/Interperiodika, Moscow.
Pasyanos, M.E., 2010. Lithospheric thickness modeled from long-period surface wave dispersion. Tectonophysics 481 (1–4), 38–50.
Pavlenkova, G.A., Pavlenkova, N.I., 2006. Upper mantle structure of the Northern Eurasia from peaceful nuclear explosion data. Tectonophysics 416 (1–4), 33–52.
Pearson, D.G., Carlson, R.W., Shirey, S.B., Boyd, F.R., Nixon, P.H., 1995. Stabilisation of Archaean lithospheric mantle; a Re–Os isotope study of peridotite xenoliths from the Kaapvaal Craton. Earth and Planetary Science Letters 134, 341–357.
Pernet-Fisher, John F., Howarth, Geoffrey H., Liu, Yang, Barry, Peter H., Carmody, Laura, Valley, John W., Bodnar, Robert J., Spetsius, Zdislav V., Taylor, Lawrence A., 2014. Komsomolskaya diamondiferous eclogites: evidence for oceanic crustal protoliths. Contributions to Mineralogy and Petrology 167, 981. http://dx.doi.org/10.1007/s00410-014-0981-y.
Pisarevsky, S.A., Natapov, L.M., 2003. Siberia and Rodinia. Tectonophysics 375, 221–245.
Pokhilenko, N.P., Sobolev, N.V., Boyd, F.R., Pearson, D.G., Shimizu, N., 1993. Megacrystalline pyrope peridotites in the lithosphere of the Siberian platform: mineralogy, geochemical peculiarities, and the problem of their origin. Russian Journal of Geology and Geophysics 34 (1), 50–62.
Pollack, H.N., Hurter, S.J., Johnson, J.R., 1993. Heat flow from the Earth's interior: analysis of the global data set. Reviews of Geophysics 31, 267–280.
Polyansky, O.P., Prokop'ev, A.V., Babichev, A.V., Korobeynikov, S.N., Reverdatto, V.V., 2013. The rift origin of the Vilyui basin (East Siberia), from reconstructions of sedimentation and mechanical mathematical modeling. Russian Geology and Geophysics 54, 121–137.
Poudjom Djomani, Y.H., O'Reilly, S.Y., Griffin, W.L., Morgan, P., 2001. The density structure of subcontinental lithosphere through time. Earth and Planetary Science Letters 184, 605–621.
Poudjom Djomani, Y.H., O'Reilly, S.Y., Griffin, W.L., Natapov, L.M., Erinchek, Y., Hronsky, J., 2003. Upper mantle structure beneath eastern Siberia: evidence from gravity modeling and mantle petrology. Geochemistry, Geophysics, Geosystems 4 (7), 1066. http://dx.doi.org/10.1029/2002GC000420.
Priestley, K., Debayle, E., 2003. Seismic evidence for a moderately thick lithosphere beneath the Siberian platform. Geophysical Research Letters 30. http://dx.doi.org/10.1029/2002GL015931.
Priestley, K., Cipar, J., Egorkin, A., Pavlenkova, N., 1994. Upper mantle velocity structure beneath the Siberian platform. Geophysical Journal International 118, 369–378.
Priestly, K., McKenzie, D., 2006. The thermal structure of the lithosphere from shear wave velocities. Earth and Planetary Science Letters 244, 285–301.
Reichow, M., Saunders, A., White, R., Pringle, M., Al'Mukhamedov, A., et al., 2002. $^{40}Ar/^{39}Ar$ dates from the West Siberian Basin: Siberian flood basalt province doubled. Science 296, 1846–1849.
Reichow, M.K., Pringle, M.S., Al'Mukhamedov, A.I., Allen, M.B., Andreichev, V.L., Buslov, M.M., Davies, C.E., Fedoseev, G.S., Fitton, J.G., Inger, S., Medvedev, A.Ya, Mitchell, C., Puchkov, V.N., Safonova, I.Yu, Scott, R.A., Saunders, A.D., 2009. The timing and extent of the eruption of the Siberian Traps large igneous province: implications for the end-Permian environmental crisis. Earth and Planetary Science Letters 277, 9–20.
Rogers, J.J.W., Santosh, M., 2002. Configuration of Columbia, a Mesoproterozoic supercontinent. Gondwana Research 5, 5–22.
Romanyuk, T., 1995. Seismic-density modeling of the crust and upper-mantle along the geotraverse QUARTZ. Izvestiya Physics of the Solid Earth (Fizika Zemli) 9, 11–23 (in Russian, English, translation available).
Rosen, O.M., 2003. The Siberian Craton: tectonic zonation and stages of evolution. Geotectonics 37 (3), 175–192.
Rosen, O.M., Condie, K.C., Natapov, L.M., Nozhkin, A.D., 1994. Archean and Early Proterozoic evolution of the Siberian Craton: a preliminary assessment. In: Condie, K.C. (Ed.), Archean Crustal Evolution. Elsevier, Amsterdam, pp. 411–459.
Rosen, O.M., Zhuravlev, D.Z., Sukhanov, M.K., Bibikova, E.V., Zlobin, V.L., 2000. Early Proterozoic terranes, collision zones, and associated anorthosites in the northeast of the Siberian Craton: isotope geochemistry and age characteristics. Russian Geology and Geophysics 41 (2), 163–180.
Schaeffer, A.J., Lebedev, S., 2013a. Global heterogeneity of the lithosphere and underlying mantle: a seismological appraisal based on multimode surface-wave dispersion analysis, shear-velocity tomography, and tectonic regionalization. The Earth's Heterogeneous Mantle. Springer Monograph (http://www.dias.ie/_aschaeff).
Schaeffer, A.J., Lebedev, S., 2013b. Global shear-speed structure of the upper mantle and transition zone. Geophysical Journal International 194, 417–449.
Semprich, J., Simon, N.S.C., Podladchikov, Yu., 2010. Density variations in the thickened crust as a function of pressure, temperature, and composition. International Journal of Earth Sciences http://dx.doi.org/10.1007/s00531-010-0557-7.
Sklyarov, E.V., Gladkochub, D.P., Mazukabzov, A.M., Stanevich, M.A., Donskaya, T.V., Konstantinov, K.M., Sinzov, A.V., 2001. Indicator complexes of supercontinent Rodinia break up. Geological Excursion Guide of Workshop 'Supercontinents and Geological Evolution of Precambrian'. Institute of the Earth Crust SB RAS, Irkutsk (75 pp. (in Russian)).
Snyder, G.A., Taylor, L.A., Crozaz, G., Halliday, A.N., Beard, B.L., Sobolev, V.N., Sobolev, N.V., 1997. The origins of Yakutian eclogite xenoliths. Journal of Petrology 38, 85–113.
Sobolev, V.N., Taylor, I.A., Snyder, G.A., Sobolev, N.V., 1994. Diamondiferous eclogites from the Udachnaya kimberlites pipe, Yakutiya,Siberia. International Geology Review 36, 42–64.
Suvorov, D., Mishen'kina, Z.R., Melnik, E.A., 2010. Upper mantle roots of Siberian Craton basement structures along the Rift DSS profile. Russian Geology and Geophysics 51, 885–897.
Villaseñor, A., Ritzwoller, M., Levshin, A., et al., 2001. Shear velocity structure of central Eurasia from inversion of surface wave velocities. Physics of the Earth and Planetary Interiors 123, 169–184.
Vyssotskiy, A.V., Vyssotski, V.N., Nezhdanov, A.A., 2006. Evolution of the West Siberian basin. Marine and Petroleum Geology 23, 93–126.
Wooden, J.L., Czamanske, G.K., Fedorenko, V.A., Arndt, N.T., Chauvel, C., Bouse, R.M., King, B.-S.W., Knigth, R.J., Siems, D., 1993. Isotopic and trace-element constraints on mantle and crustal contribution to Siberian continental flood basalts, Noril'sk area, Siberia. Geochimica et Cosmochimica Acta 57, 3677–3704.
Yang, X., Yang, Y., Chen, J., 2014. Pressure dependence of density, porosity, compressional wave velocity of fault rocks from the ruptures of the 2008 Wenchuan earthquake, China. Tectonophysics 619–620, 133–142.
Yegorova, T., Pavlenkova, G., 2014. Structure of the upper mantle of Northern Eurasia from 2D density modeling on seismic profiles with peaceful nuclear explosions. Tectonophysics 627, 57–71.
Zhao, G., Cawood, P.A., Wilde, S.A., Sun, M., 2002. Review of global 2.1–1.8 Ga orogens: implications for a pre-Rodinia supercontinent. Earth-Science Reviews 59 (1–4), 125–162.
Zonenshain, L.P., Kogan, L.I., Savostin, L.A., Golmstock, A.Ja., Gorodnitskii, A.M., 1980. Tectonic, crustal structure and evolution of the Galapagos triple junction. Marine Geology 37, 209–230.
Zonenshain, L.P., Kuzmin, M.I., Natapov, L.M., 1990. Geology of the USSR: A Plate-Tectonic Synthesis. Geodynamics Series, 21. AGU, Washington, D.C. (242 pp.).